AIMS Mathematics, 9(5): 11596–11621.
DOI: 10.3934/math.2024569
Received: 07 January 2024
Revised: 05 February 2024
Accepted: 01 March 2024
Published: 25 March 2024

http://www.aimspress.com/journal/Math

Research article

Piecewise immunosuppressive infection model with viral logistic growth and effector cell-guided therapy

Xiong Zhang[1] **and Zhongyi Xiang**[1,2,*]

[1] School of Mathematics and Statistics, Hubei Minzu University, Enshi, Hubei 445000, China
[2] Hubei Key Laboratory of Selenium Resource Research and Biological Application, Hubei Minzu University, Enshi, Hubei 445000, China

* **Correspondence:** Email: yfxiang2007@163.com.

Abstract: This work investigated a piecewise immunosuppressive infection model that assessed the effectiveness of implementing this therapeutic regimen once the effector cell count falls below a specific threshold level by introducing a threshold strategy. The sliding mode dynamics, global dynamics, and boundary equilibrium bifurcations of the Filippov system were examined based on the global dynamics of the two subsystems. Our primary findings indicate that the HIV viral loads and effector cell counts can be stabilized within the required predetermined level. This outcome depends on the threshold level, immune intensity, and the initial values of the system. Therefore, properly combining these key factors makes it possible to effectively curb the abnormal increase of virus and keep the effector cells at a reliable level. This approach maximizes the controllable range of the HIV. The proposed switching system incorporating pseudo-equilibrium exhibits three types of equilibriums that could be bistable or tristable. It means there is a possibility of controlling the virus after administering therapy if the immune intensity c is limited within the range of the post-treatment control threshold and the elite control threshold when $R_0 > R_{c_1} > R_{c_2} > 1$.

Keywords: immunosuppressive infection model; Filippov system; sliding mode; immune intensity; global dynamics
Mathematics Subject Classification: 34D05, 34D23, 92C60

1. Introduction

Epidemics have posed a significant threat to global public health over the years. The emergence of COVID-19 in 2019 has had a profound impact on human health, the global economy, and social behavior. Nevertheless, the effective addressing of disease transmission remains a challenge. Mathematical modeling has emerged as a crucial tool in tackling this challenge. Numerous disease

models have been developed in existing literature to study and control the spread of epidemics. It is important to note that mathematical models based on ordinary differential equations (i.e., classical derivatives) have their limitations and may not accurately capture biological phenomena. On the other hand, fractional models can offer a relatively more accurate understanding of disease outbreaks. Therefore, they are increasingly being used to simulate disease transmission with higher accuracy. Relevant literature on fractional models can be found in [1–5]. In addition, as another epidemic that endangers human health, the acute viral infection caused by the human immunodeficiency virus (HIV) studied in this paper is also a hot issue in society. Many researchers aim to capture the dynamics between viral and antiviral immune responses through mathematical modeling.

As we all know, HIV, which causes AIDS, can directly infect the immune system (mainly regulating $CD4^+$ T cells). The consequences of this impact are a continuous decrease in the number of $CD4^+$ T cells, ultimately leading to the death of infected individuals due to immune system collapse. The highly active antiretroviral therapy (HAART) currently in widespread use has been shown to improve the survival probability of HIV patients and reduce the incidence rate [6, 7]. This therapy effectively suppresses the plasma virus to levels below the standard detection for extended periods and even halts viral evolution [8,9]. However, many complex problems arise after long-term use, such as obvious drug resistance, and, due to the side effects of antiviral drugs, some AIDS patients have poor compliance with antiviral therapy [10–12].

In fact, numerous mathematical models have been put forth to describe the dynamics of HIV and elucidate various phenomena. The effect of antiviral therapy has been investigated by some researchers [13–16]. In their work, Xiao et al. [13] analyzed the free terminal time optimal tracking control problem to determine the optimal multidrug therapy for HIV, considering both the optimal time frame and therapeutic strategies. The literature [17–24] incorporated the expansion delay of immune cells to discuss the local and global stability of equilibrium solutions. In particular, [17] indicates that such an unstable equilibrium will exhibit oscillatory solutions of increasing amplitude. In recent years, realizing gradually the multiple effects of spatial heterogeneity and mobility, many scholars utilized the reaction-diffusion equation to investigate the spatial effect of viral infection [23–25].

Several recent clinical studies have exhibited that structured treatment interruptions (STIs) can be used for early treatment of HIV infection to achieve sustained specific immunity. For some chronically infected individuals who may require lifelong medication, this may be a beneficial option as it can help patients rebuild their immune system during periods of non-medication [26]. While numerous mathematical models have been employed for simulating continuous therapy [27–29], there is scant investigation on modeling structured interruptions in treatment.

To investigate strategies for STIs, Tang et al. [30] suggested a piecewise model for delineating CD4 cell-guided STIs. The system provides an explanation for some controversial clinical research results. In 2017, Tang et al. [31] proposed a mathematical model to describe the dynamics of the interplay between the virus and the immune system. This model takes into consideration the structured treatment guided by effector cells while also incorporating the use of combined antiretroviral therapy and interleukin (IL)-2 treatment. However, they posit a linear growth pattern for the HIV virus [31], which does not accurately reflect the true dynamics of the virus. Some clinical facts show that the growth of HIV may have a saturation effect [32].

To better illustrate the non-linear evolutionary characteristics of the interplay between virus and immune response, the immunosuppressive infection model was devised by Komarova et al. [33]. The

model is given as follows:

$$\begin{cases} \frac{dy}{dt} = ry\left(1-\frac{y}{K}\right) - ay - pyz, \\ \frac{dz}{dt} = \frac{cyz}{1+\eta y} - bz - qyz, \end{cases} \tag{1.1}$$

The assumptions in model (1.1) are as follows:

- y and z represent the population sizes of the virus and immune cells, respectively. The virus population is assumed to grow logistically: The replication rate at low viral loads, denoted as r, is expected to decrease linearly with an increase in the viral load until it becomes zero at a viral load K.
- c represents the immune intensity, while the proliferation term is denoted as $cyz/(1+\eta y)$. Thus, the assessment of immune cell proliferation depends on both the immune cells and the virus. The inhibitory effect of the virus on the proliferation of immune cells is represented by the variable η.
- The viral elimination rate, denoted as a, is a result of natural decay and antiretroviral therapy. Immune cells, which have the ability to kill the virus at a rate pyz, also have a death rate b. Furthermore, these immune cells can be inhibited by the virus at a rate qyz.

The study conducted in [33] aimed to investigate the optimal timing and duration of antiviral treatment. The research elucidates the presence of bistability dynamics, wherein a stable state without immunity coexists alongside a stable state with immunity. Meanwhile, this model demonstrates the attainment of sustained immunity following the interruption of therapy. Additionally, Wang et al. [34] expanded on this model and uncovered that bistability arises within the range delineated by the post-treatment control threshold and the elite control threshold.

Following the pioneer works above [30–34], in this thesis, we extend model (1.1) by proposing a Filippov immunosuppressive infection model with viral logistic growth and effector cell-guided therapy. We have proposed the following model:

$$\begin{cases} \left.\begin{aligned} \frac{dy}{dt} &= ry\left(1-\frac{y}{K}\right) - ay - pyz, \\ \frac{dz}{dt} &= \frac{cyz}{1+\eta y} - bz - qyz, \end{aligned}\right\} z > E_T, \\ \left.\begin{aligned} \frac{dy}{dt} &= ry\left(1-\frac{y}{K}\right) - ay - pyz, \\ \frac{dz}{dt} &= \frac{cyz}{1+\eta y} - bz - qyz + \varepsilon z, \end{aligned}\right\} z < E_T. \end{cases} \tag{1.2}$$

We assume that the sole course of action is to administer antiretroviral therapy to the patient if the number of effector cells exceeds the critical value E_T. Conversely, when the count falls below the E_T threshold, a combination of antiretroviral therapy and immune therapy is concurrently implemented. In this context, ε represents the rate at which effector cells grow as a result of immune therapy, like the treatment of interleukin (IL)-2. As the interpretation of other parameters is consistent with a model (1.1), all parameters in (1.2) remain nonnegative.

This paper presents a switching model with viral load logistic growth to analyze effector cell-guided treatment and assess the threshold strategy's effectiveness. The following section provides an overview of the model, defining the switching system, and summarizing the dynamic behavior of the subsystems. Additionally, in Section 3, there is a discussion on sliding mode and dynamics, exploring the presence of a sliding domain and pseudo-equilibrium. The global dynamics of the proposed model are examined in Section 4, while Section 5 focuses on the boundary equilibrium bifurcation of the system. Finally, the paper concludes with discussions and biological implications.

2. Filippov model and preliminaries

2.1. Model formulation

By rearranging the system (1.2), we can obtain a generic planar system in the form of Filippov given by

$$\begin{cases} \frac{dy}{dt} = ry\left(1-\frac{y}{K}\right) - ay - pyz, \\ \frac{dz}{dt} = \frac{cyz}{1+\eta y} - bz - qyz + \phi\varepsilon z, \end{cases} \tag{2.1}$$

with

$$\begin{cases} \phi = 0, \quad if H(X) = z - E_T > 0, \\ \phi = 1, \quad if H(X) = z - E_T < 0. \end{cases} \tag{2.2}$$

Systems (2.1) and (2.2) describe a Filippov immunosuppressive infection model where (2.1) is considered a free system when $\phi = 0\,(i.e., z > E_T)$, indicating that the patient receives antiretroviral therapy. On the other hand, (2.1) as a control system when $\phi = 1\,(i.e., z < E_T)$ reflects the simultaneous utilization of antiretroviral therapy and immune therapy.

Let $R^2_+ = \left\{ X = (y,z)^T \middle| y \geqslant 0, z \geqslant 0 \right\}$, $S^1 = \left\{ X \in R^2_+ \middle| H(X) > 0 \right\}$, and $S^2 = \left\{ X \in R^2_+ \middle| H(X) < 0 \right\}$ with $H(X)$ being a smooth scale function. For convenience, we further denote

$$\begin{aligned} F_{S^1}(X) &= \left(ry\left(1-\tfrac{y}{K}\right) - ay - pyz, \tfrac{cyz}{1+\eta y} - bz - qyz \right)^T, \\ F_{S^2}(X) &= \left(ry\left(1-\tfrac{y}{K}\right) - ay - pyz, \tfrac{cyz}{1+\eta y} - bz - qyz + \varepsilon z \right)^T. \end{aligned} \tag{2.3}$$

We can rewrite model (1.2) to represent the Filippov system as follows:

$$\dot{X} = \begin{cases} F_{S^1}(X),\ X \in S^1, \\ F_{S^2}(X),\ X \in S^2. \end{cases} \tag{2.4}$$

The discontinuous boundary Σ that separates the two areas can be represented as:

$$\Sigma = \left\{ X \in R^2_+ \middle| H(X) = 0 \right\}. \tag{2.5}$$

It is evident that $R^2_+ = S^1 \cup \Sigma \cup S^2$. Henceforth, we shall designate the Filippov system (2.4) as subsystem $\mathbb{S}^1$ when it is defined within region S^1, and as subsystem $\mathbb{S}^2$ when defined within region S^2.

Let

$$\sigma(X) = \langle H_X(X), F_{S^1}(X) \rangle \cdot \langle H_X(X), F_{S^2}(X) \rangle = F_{S^1}H(X) \cdot F_{S^2}H(X), \tag{2.6}$$

where $\langle \cdot, \cdot \rangle$ represents the standard scalar product and $H_X(X)$ denotes the gradient of $H(X)$ that remains nonvanishing on Σ. $F_{S^i}H(X) = F_{S^i} \cdot \mathrm{grad}H(X)$ is the Lie derivative of H with respect to the vector field F_{S^i} $(i = 1,2)$ at X. To analyze the direction of the vector field $[F_{S^1}(X), F_{S^2}(X)]$, through a specific point $X \in \Sigma$, we categorize the areas on Σ based on whether the vector field points towards it:

(a) Crossing region:

$$\Sigma_c = \{ X \in \Sigma | F_{S^1}H(X) \cdot F_{S^2}H(X) > 0 \}, \tag{2.7}$$

(b) Sliding region:

$$\Sigma_s = \{ X \in \Sigma | F_{S^1}H(X) < 0, F_{S^2}H(X) > 0 \}, \tag{2.8}$$

(c) Escaping region:

$$\Sigma_e = \{X \in \Sigma | F_{S^1}H(X) > 0, F_{S^2}H(X) < 0\}. \tag{2.9}$$

Throughout the paper, it is crucial to have a clear understanding of the definitions regarding all types of equilibria in Filippov systems [35, 36].

Definition 2.1. *If $F_{S^1}(X_*) = 0, H(X_*) > 0$, or $F_{S^2}(X_*) = 0$, $H(X_*) < 0$, then X_* is defined as a real equilibrium of the Filippov system* (2.4)*. Analogously, if $F_{S^1}(X_*) = 0$, $H(X_*) < 0$, or $F_{S^2}(X_*) = 0, H(X_*) > 0$, then X_* is a virtual equilibrium. Both the real and virtual equilibriums are named as regular equilibria.*

Definition 2.2. *If X_* is an equilibrium of the sliding mode of system* (2.4)*, and satisfies $(1-\lambda)F_{S^1}(X_*) + \lambda F_{S^2}(X_*) = 0, H(X_*) = 0$ with $0 < \lambda < 1$, then X_* is a pseudo-equilibrium, where*

$$\lambda = \frac{\langle H_X(X_*), F_{S^1}(X_*)\rangle}{\langle H_X(X_*), F_{S^1}(X_*) - F_{S^2}(X_*)\rangle}. \tag{2.10}$$

Definition 2.3. *If $F_{S^1}(X_*) = 0, H(X_*) = 0$, or $F_{S^2}(X_*) = 0, H(X_*) = 0$, then X_* is defined a boundary equilibrium of Filippov system* (2.4)*.*

Definition 2.4. *If $F_{S^1}H(X_*) = 0$ but $F^2_{S^1}H(X_*) > 0 \left(F^2_{S^1}H(X_*) < 0\right)$, then X_* is a visible (invisible) Σ-fold point of F_{S^1}. The same definition applies to F_{S^2}.*

Definition 2.5. *If $X_* \in \Sigma_s$ and $F_{S^1}H(X_*) = 0$ or $F_{S^2}H(X_*) = 0$, then X_* is defined a tangent point of Filippov system* (2.4)*.*

2.2. Qualitative analysis of subsystems

The model equation for the free system $\mathbb{S}^1$ is as follows:

$$\begin{cases} \frac{dy}{dt} = ry\left(1 - \frac{y}{K}\right) - ay - pyz, \\ \frac{dz}{dt} = \frac{cyz}{1+\eta y} - bz - qyz. \end{cases} \tag{2.11}$$

We can easily define a threshold $R_0 = \frac{r}{a}$. If $R_0 < 1$, subsystem $\mathbb{S}^1$ has only one uninfected equilibrium $E_0^1 = (0,0)$; if $R_0 > 1$, then subsystem $\mathbb{S}^1$ also has an immune-free equilibrium $E_1^1 = (y_1, 0) = \left(K\left(1 - \frac{a}{r}\right), 0\right)$.

We certainly get an equation for y

$$S_1(y) = q\eta y^2 - (c - q - b\eta)y + b = 0, \tag{2.12}$$

It can be confirmed that $S_1(y) = 0$ has a sole solution when $c = q + b\eta \pm 2\sqrt{bq\eta}$. Denote $c_1 = q + b\eta - 2\sqrt{bq\eta}$ and $c_2 = q + b\eta + 2\sqrt{bq\eta}$. Thus, we have two possible positive roots

$$y_{11} = \frac{B - \sqrt{B^2 - 4bq\eta}}{2q\eta}, y_{12} = \frac{B + \sqrt{B^2 - 4bq\eta}}{2q\eta}, \tag{2.13}$$

when $c > c_2$, where $B = c - q - b\eta$. Substituting y_{11} or y_{12} into the first equation of (2.11), we get

$$z_{1i} = \frac{r\left(1 - \frac{y_{1i}}{K}\right) - a}{p} = \frac{a\left[\frac{r}{a}\left(1 - \frac{y_{1i}}{K}\right) - 1\right]}{p} \, (i = 1, 2). \tag{2.14}$$

Let $R_i^1 = \frac{r}{a}\left(1-\frac{y_{1i}}{K}\right)(i=1,2)$. Hence, the subsystem $\mathbb{S}^1$ has two immune equilibriums $E_{11} = (y_{11}, z_{11})$ and $E_{12} = (y_{12}, z_{12})$ when $R_i^1 > 1$ and $c > c_2$ are satisfied.

In fact, subsystem $\mathbb{S}^1$ has been extensively examined in a previous study. Therefore, we will provide an overview of the main findings without delving into specific calculations. For more details on the discussion of the stability analysis of this system, please consult [34]. Here, we define three thresholds by referring [34], i.e., $c^*=q+b\eta+2q\eta K\left(1-\frac{a}{r}\right)$, $c^{**}=q+b\eta+\frac{b}{K\left(1-\frac{a}{r}\right)}+q\eta K\left(1-\frac{a}{r}\right)$, and threshold $R_{c_1} = 1+\frac{r\sqrt{bq\eta}}{aq\eta K}$. Moreover, we have the following

Lemma 2.1. *If $R_0 < 1$, the infection-free equilibrium E_0^1 is globally asymptotically stable (GAS). If $R_0 > 1$, we have E_1^1 as locally asymptotically stable (LAS) when $0 < c < c_2$ or $c_2 < c < c^{**}$, and E_1^1 is unstable when $c > c^{**}$. The immune equilibrium E_{11} is LAS when $R_{c_1} > R_0 > 1$ and $c > c^{**}$ or $R_0 > R_{c_1}$ and $c_2 < c$. Suppose $R_0 > R_{c_1} > 1$ and $c_2 < c < c^*$, then positive equilibrium E_{11} is LAS and E_{12} is a unstable saddle.*

Remark 2.1. *For $R_0 > R_{c_1} > 1$ and $c_2 < c < c^{**}$, subsystem $\mathbb{S}^1$ has bistable behavior, i.e., E_1^1 and E_{11} are bistable but the equilibrium E_{12} is an unstable saddle. In other cases, subsystem $\mathbb{S}^1$ does not exhibit bistable behavior. Note that the post-treatment control threshold is represented by c_2, while the elite control threshold is denoted as c^{**}. The range between c_2 and c^{**} is referred to as the bistable interval.*

Dynamical analysis of the subsystem $\mathbb{S}^1$ is presented in Table 1.

Table 1. Dynamical analysis of the subsystem $\mathbb{S}^1$.

Condition	E_0^1	E_1^1	E_{11}	E_{12}	subsystem $\mathbb{S}^1$
$R_0 < 1$	*GAS*	–	–	–	Asymptotically tends to E_0^1
$R_0 > 1, 0 < c < c_2$	*US*	*LAS*	–	–	Asymptotically tends to E_1^1
$R_0 > R_{c_1} > 1, c_2 < c < c^{**}$	*US*	*LAS*	*LAS*	*US*	Bistable
$R_0 > R_{c_1} > 1, c^{**} < c < c^*$	*US*	*US*	*LAS*	*US*	Asymptotically tends to E_{11}
$R_0 > R_{c_1} > 1, c^* < c$	*US*	*US*	*LAS*	–	Asymptotically tends to E_{11}
$R_{c_1} > R_0 > 1, 0 < c < c^{**}$	*US*	*LAS*	–	–	Asymptotically tends to E_1^1
$R_{c_1} > R_0 > 1, c^{**} < c$	*US*	*US*	*LAS*	–	Asymptotically tends to E_{11}

Control system $\mathbb{S}^2$ gives

$$\begin{cases} \frac{dy}{dt} = ry\left(1-\frac{y}{K}\right) - ay - pyz, \\ \frac{dz}{dt} = \frac{cyz}{1+\eta y} - bz - qyz + \varepsilon z. \end{cases} \tag{2.15}$$

The basic reproduction number is also $R_0 = \frac{r}{a}$ for subsystem $\mathbb{S}^2$. Similarly, we can get uninfected equilibrium $E_0^2 = (0,0)$ and the immune-free equilibrium $E_1^2 = \left(K\left(1-\frac{a}{r}\right), 0\right)$. Thus, we use $E_0^1 = E_0^2 = E_0$ and $E_1^2 = E_1^1 = E_1$ in the following.

Using the same method as subsystem $\mathbb{S}^1$, we can derive the following quadratic equation for y

$$S_2(y) = q\eta y^2 - (c - q - b\eta + \varepsilon\eta)y + b - \varepsilon = 0. \tag{2.16}$$

Let $c_3 = q + (b-\varepsilon)\eta - 2\sqrt{q\eta(b-\varepsilon)}$ and $c_4 = q + (b-\varepsilon)\eta + 2\sqrt{q\eta(b-\varepsilon)}$, then there are two possible positive roots

$$y_{2i} = \frac{D \mp \sqrt{D^2 - 4q\eta(b-\varepsilon)}}{2q\eta}(i = 1,2), \tag{2.17}$$

when $c > c_4$, where $D = c - q - b\eta + \varepsilon\eta$. It follows that

$$z_{21} = \frac{a\left[\frac{r}{a}\left(1 - \frac{y_{21}}{K}\right) - 1\right]}{p}, z_{22} = \frac{a\left[\frac{r}{a}\left(1 - \frac{y_{22}}{K}\right) - 1\right]}{p}. \tag{2.18}$$

In fact, we can obtain $y_{21} < y_{11} < y_{12} < y_{22}$ by doing a simple calculation. Now, we define $R_i^2 = \frac{r}{a}\left(1 - \frac{y_{2i}}{K}\right)(i = 1,2)$. For subsystem $\mathbb{S}^2$, we have two positive equilibriums $E_{21} = (y_{21}, z_{21})$ and $E_{22} = (y_{22}, z_{22})$ when $c > c_4$, $b > \varepsilon$ and $R_i^2 > 1\,(i = 1,2)$ hold. Furthermore, following a similar approach to subsystem $\mathbb{S}^1$, we can also define thresholds $c^{\dagger} = q + (b-\varepsilon)\eta + 2q\eta K\left(1 - \frac{a}{r}\right)$, $c^{\dagger\dagger} = q + (b-\varepsilon)\eta + \frac{b-\varepsilon}{K\left(1-\frac{a}{r}\right)} + q\eta K\left(1 - \frac{a}{r}\right)$, and $R_{c_2} = 1 + \frac{r\sqrt{q\eta(b-\varepsilon)}}{aq\eta K}$. Meanwhile, we have the following results about the behaviors of subsystem $\mathbb{S}^2$ by using the consistent method with $\mathbb{S}^1$.

Lemma 2.2. *Suppose $R_0 < 1$, the equilibrium E_0^2 is GAS. Suppose $R_0 > 1$, then E_1^2 is LAS when $0 < c < c_4$ or $c_4 < c < c^{\dagger\dagger}$, and E_1^2 is unstable when $c > c^{\dagger\dagger}$. If $R_{c_2} > R_0 > 1$ and $c > c^{\dagger\dagger}$ or $R_0 > R_{c_2}$ and $c_4 < c$, the subsystem $\mathbb{S}^2$ has a locally asymptotically stable immune equilibrium E_{21}; if $R_0 > R_{c_2} > 1$ and $c_4 < c < c^{\dagger}$, then positive equilibrium E_{21} is LAS and E_{22} is an unstable saddle.*

Dynamical analysis of the subsystem $\mathbb{S}^2$ is shown in Table 2.

Table 2. Dynamical analysis of the subsystem $\mathbb{S}^2$.

Condition	E_0^2	E_1^2	E_{21}	E_{22}	subsystem $\mathbb{S}^2$
$R_0 < 1$	*GAS*	–	–	–	Asymptotically tends to E_0^2
$R_0 > 1, 0 < c < c_4$	*US*	*LAS*	–	–	Asymptotically tends to E_1^2
$R_0 > R_{c_2} > 1, c_4 < c < c^{\dagger\dagger}$	*US*	*LAS*	*LAS*	*US*	Bistable
$R_0 > R_{c_2} > 1, c^{\dagger\dagger} < c < c^{\dagger}$	*US*	*US*	*LAS*	*US*	Asymptotically tends to E_{21}
$R_0 > R_{c_2} > 1, c^{\dagger} < c$	*US*	*US*	*LAS*	–	Asymptotically tends to E_{21}
$R_{c_2} > R_0 > 1, 0 < c < c^{\dagger\dagger}$	*US*	*LAS*	–	–	Asymptotically tends to E_1^2
$R_{c_2} > R_0 > 1, c^{\dagger\dagger} < c$	*US*	*US*	*LAS*	–	Asymptotically tends to E_{21}

3. Sliding mode dynamics

In this section, we will provide a brief overview of the definitions pertaining to the sliding segment and crossing segment discussed in Section 2. We have $\sigma(X) = \langle H_X(X), F_{S^1}(X)\rangle \cdot \langle H_X(X), F_{S^2}(X)\rangle$. Here, $H_X(X) = \left(\frac{\partial H}{\partial y}, \frac{\partial H}{\partial z}\right)$ is the non-vanishing gradient on the discontinuity boundary Σ, where $H = z - E_T$. Therefore, we denote

$$\sigma(X) = \left(\frac{cyz}{1+\eta y} - bz - qyz\right)\left(\frac{cyz}{1+\eta y} - bz - qyz + \varepsilon z\right), \tag{3.1}$$

and calculating the inequality $\sigma(X) < 0$ obtains $y_{21} < y < y_{11}$ and $y_{12} < y < y_{22}$. Naturally, we can verify that there are $\langle F_{S^1}, H_X(X)\rangle = \frac{cyz}{1+\eta y} - bz - qyz < 0$ and $\langle F_{S^2}, H_X(X)\rangle = \frac{cyz}{1+\eta y} - bz - qyz + \varepsilon z > 0$ for $y_{21} < y < y_{11}$ or $y_{12} < y < y_{22}$. Therefore, the Filippov system (2.4) always comprises two sliding segments, which can be obtained as

$$\Sigma_s^1 = \left\{ (y,z) \in R_+^2 \middle| y_{21} < y < y_{11}, z = E_T \right\}, \Sigma_s^2 = \left\{ (y,z) \in R_+^2 \middle| y_{12} < y < y_{22}, z = E_T \right\}. \tag{3.2}$$

Naturally, the crossing region we can get is $\Sigma_c = \left\{ (y,z) \in R_+^2 \middle| 0 < y < y_{21}, \text{ or } y_{11} < y < y_{12}, \text{ or } y > y_{22}, z = E_T \right\}$. Notably, every trajectory within the segment $\left\{ (y,z) \in R_+^2 \middle| 0 < y < y_{21} \text{ or } y > y_{22}, z = E_T \right\}$ will intersect the $z = E_T$ line, moving from region S^1 to S^2. Similarly, the trajectory within the segment $\left\{ (y,z) \in R_+^2 \middle| y_{11} < y < y_{12}, z = E_T \right\}$ will cross the $z = E_T$ line, transitioning from region S^2 to S^1.

The Filippov convex method is employed in this study to analyze the sliding domain and sliding mode dynamics of the switching system (2.4). According to Definition 2.2, we have

$$\frac{dX}{dt} = F_S(X) = (1-\lambda) F_{S^1}(X) + \lambda F_{S^2}(X). \tag{3.3}$$

By a straightforward calculation, one can get

$$\langle H_X, F_{S^1}(X)\rangle = \frac{cyz}{1+\eta y} - bz - qyz, \langle H_X, F_{S^1}(X) - F_{S^2}(X)\rangle = -\varepsilon z. \tag{3.4}$$

It follows that

$$\lambda = \frac{\frac{cyz}{1+\eta y} - bz - qyz}{-\varepsilon z} = \frac{q\eta y^2 - (c-q-b\eta) y + b}{\varepsilon (1+\eta y)}. \tag{3.5}$$

Therefore, the dynamic equation of the switching system (2.4) on the sliding mode domain is

$$\begin{cases} \frac{dy}{dt} = ry\left(1 - \frac{y}{K}\right) - ay - pyE_T, \\ \frac{dz}{dt} = 0. \end{cases} \tag{3.6}$$

There exists one positive equilibrium $E_c = (y_c, E_T)$, where $y_c = K\left(1 - \frac{a+pE_T}{r}\right)$. We can easily obtain that $r > a + pE_T$. According to Definition 2.2, the equilibrium E_c is referred to as a pseudo-equilibrium.

When $y_{21} < y_c < y_{11}$, we have

$$y_{11} - y_c = \frac{rB - r\sqrt{B^2 - 4qb\eta} - 2q\eta Kr + 2q\eta K(a + pE_T)}{2q\eta r} > 0, \tag{3.7}$$

and

$$y_c - y_{21} = \frac{2q\eta K[r - (a + pE_T)] - r\left(D - \sqrt{D^2 - 4q\eta(b-\varepsilon)}\right)}{2q\eta r} > 0. \tag{3.8}$$

Clearly, $y_{21} < y_c < y_{11}$ is equivalent to

$$\frac{r-a}{p} - \frac{r\left(B - \sqrt{B^2 - 4qb\eta}\right)}{2qp\eta K} < E_T < \frac{r-a}{p} - \frac{r\left(D - \sqrt{D^2 - 4q\eta(b-\varepsilon)}\right)}{2qp\eta K}, \tag{3.9}$$

$(i.e., z_{11} < E_T < z_{21})$. Thus, the equilibrium E_c is located on the sliding segment Σ_s^1 when $z_{11} < E_T < z_{21}$. It can be readily confirmed that $dy/dt < 0$ holds on the segment Σ_s^2. Similariy, if $y_{12} < y_c < y_{22}$, we conclude that

$$\frac{r-a}{p} - \frac{r\left(D+\sqrt{D^2-4q\eta\,(b-\varepsilon)}\right)}{2qp\eta K} < E_T < \frac{r-a}{p} - \frac{r\left(B+\sqrt{B^2-4qb\eta}\right)}{2qp\eta K}, \tag{3.10}$$

$(i.e., z_{22} < E_T < z_{12})$. Under this circumstance, the pseudo-equilibrium E_c is located on the sliding segment $\Sigma_s^2 = \{(y,z)|\, y_{12} < y < y_{22}, z = E_T\}$ for $z_{22} < E_T < z_{12}$, meanwhile, we can get $dy/dt > 0$ holds on the segment Σ_s^1.

Theorem 3.1. *If $z_{11} < E_T < z_{21}$, system(2.4) has one pseudo-equilibrium $E_c = \left(K\left(1-\frac{a+pE_T}{r}\right), E_T\right)$ on the sliding segment Σ_s^1, which is always LAS when it exists; analogously, if $z_{22} < E_T < z_{12}$, then pseudo-equilibrium E_c is LAS on the sliding segment Σ_s^2.*

Proof. Without loss of generality, we only consider the proof for the first case. Let $y' = ry\left(1-\frac{y}{K}\right) - ay - pyz \doteq g(y)$. Substituting $H = z - E_T = 0$ into the $g(y)$, we will get $g(y) = -\frac{r}{K}y^2 + (r-a-pE_T)\,y$. Based on the function $g(y)$, we know $g(y_{21}) > 0, g(y_{11}) < 0$. Further, we note that $y' = g(y)$, then $g'(y) = -\frac{2r}{K}y + (r-a-pE_T)$. Naturally $g'(y_c) = -\frac{2r}{K}\cdot K\left(1-\frac{a+pE_T}{r}\right) + (r-a-pE_T) = -r+a+pE_T < 0$, which implies that E_c is *LAS*. Thus, the equilibrium E_c is locally stable provided it is feasible. Likewise, we can use a similar method to prove E_c is *LAS* on the Σ_s^2.

4. Global dynamics of system (2.3)

This part focuses on examining the global dynamics of a switching system. To certify the global stability of the equilibrium of the system (2.4), it is necessary to rule out the presence of limit cycles. Firstly, we let the Dulac function be $V(y,z) = 1/yz$. For subsystem $\mathbb{S}^i (i = 1,2)$, this gives $\frac{\partial}{\partial y}\left(V(y,z)\frac{dy}{dt}\right) + \frac{\partial}{\partial z}\left(V(y,z)\frac{dz}{dt}\right) = -\frac{r}{zK} < 0$. Based on the Dulac-Bendixson criterion, it can be concluded that there are no limit cycles present. Consequently, we can derive the following Lemma 4.1.

Lemma 4.1. *There exists no limit cycle that is entirely situated within the region $S^i (i = 1,2)$.*

Next, we will exclude limit cycles that intersect with the sliding segment or surrounding the whole sliding segment. Note that this exclusion is necessary for us to follow up with better explanations.

Lemma 4.2. *There does not exist a limit cycle that includes a portion of the sliding segment.*

Proof. We need to establish the proofs of Lemma 4.2 for the cases $E_T > z_{21}$, $z_{11} < E_T < z_{21}$, $z_{12} < E_T < z_{11}$, $z_{22} < E_T < z_{12}$, and $0 < E_T < z_{22}$.

If $E_T > z_{21}$, the absence of pseudo-equilibrium is deduced from the demonstration of Theorem 3.1, which indicates the presence of $dy/dt < 0$ on the sliding segments $\Sigma_s^i (i = 1,2)$ under such circumstances. Therefore, any trajectory reaching Σ_s^1 or Σ_s^2 will approach the boundary points (y_{21}, E_T), and E_{21} is a real stable node. Note that (y_{21}, E_T) is visible Σ-fold points of subsystem $\mathbb{S}^2$ (see Definition 2.4 in Section 2). Thus, the trajectory initiating at (y_{21}, E_T) tends to either approach the stable state E_{21} directly or in a spiral manner [shown in Figure 1(a)], without touching the switching line again. Therefore, there are no closed orbits that include any part of the sliding segment.

If $z_{11} < E_T < z_{21}$, we know that the pseudo-equilibrium E_c is *LAS* on the segment Σ_s^1 (see Theorem 3.1 in Section 3) under this scenario, which means the nonexistence of a limit cycle

that contains part of the sliding segment Σ_s^1. Beyond that, there is $dy/dt < 0$ on the segment $\{(y,z)|y_{12} < y < y_{22}, z = E_T\}$ when $z_{11} < E_T < z_{21}$. This implies that the orbits reaching sliding segment Σ_s^2 firstly slide towards the boundary point (y_{12}, E_T), which is a visible Σ-fold point as well, enter into the S^1, and then tend to E_c. Therefore, there exists no limit cycle incorporating any portion of the sliding segment.

If $z_{12} < E_T < z_{11}$, there exists one real stable equilibrium E_{11} in region S^1. Thus, we can employ a way similar to that applied in the first case to demonstrate the conclusion [shown in Figure 1(b)].

If $z_{22} < E_T < z_{12}$, we have that pseudo-equilibrium E_c is *LAS* on the sliding segment Σ_s^2. We get $dy/dt > 0$ on the segment Σ_s^1 in this case. Clearly, the proof process is similar to the second case, so we have omitted here.

If $0 < E_T < z_{22}$, we know that there is no pseudo-equilibrium, and $dy/dt > 0$ holds on the sliding segments $\Sigma_s^i\,(i = 1,2)$, since there exists a stable equilibrium E_1, and (y_{22}, E_T) is visible Σ-fold point. Thus, the orbits starting from segments $\Sigma_s^i\,(i = 1,2)$ move from the left to the right along the sliding line to the boundary point (y_{22}, E_T). Then, they proceed into region S^1 and eventually converge to E_1, without experiencing hitting the switching line $z = E_T$ again. Thus, the proof for Lemma 4.2 is thereby completed.

Significantly, the following lemma is similar to previous studies [37, 38], which is obtained by constructing a cycle around the sliding segment and then using the method of counter-evidence to draw a contradiction.

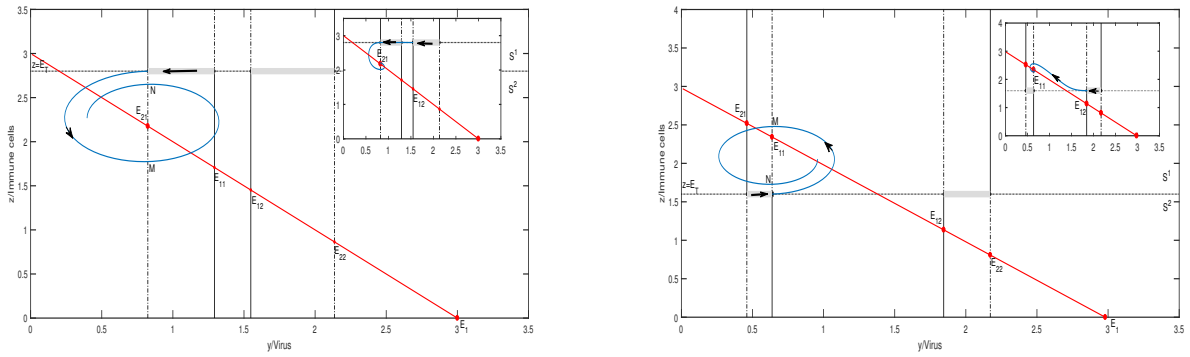

(a) (b)

Figure 1. The blue lines represent possible closed tracks that contain a portion of the sliding segment.

Lemma 4.3. *There exists no closed orbit containing the whole sliding segment.*

Combined with analysis in Section 2, we obtain the two sets of key parameters, i.e., R_0, R_{c_1}, R_{c_2}, and $c_2, c_4, c^*, c^{**}, c^{\dagger}, c^{\dagger\dagger}$. They are the crucial elements that determine the dynamic behavior of the system (2.4). Next, we will discuss the global dynamics of the proposed piecewise system based on the relationships between the parameters mentioned earlier. Considering that there exists only one uninfected equilibrium E_0 for both subsystem $\mathbb{S}^1$ and $\mathbb{S}^2$ when $R_0 < 1$, we will not delve further into it. Here, we will focus on the following situations:

Case(a): $R_0 > R_{c_1} > R_{c_2} > 1$,

Case(b): $R_{c_1} > R_{c_2} > R_0 > 1$,

Case(c): $R_{c_1} > R_0 > R_{c_2} > 1$.

4.1. The global dynamics for Case (a)

The global dynamics for Case (a) are the main focus of this section. Note that the analysis methods for the three cases are analogous, thus we have omitted detailed proofs for the other cases. According to the results in Section 2, it can be seen that the relationship between immune intensity c and parameters $c_2, c_4, c^*, c^{**}, c^{\dagger}, c^{\dagger\dagger}$ have a significant impact on the dynamics of the system (2.4). Through direct analysis, we will consider the under situations:

$$c_4 < c < c_2; c_2 < c < c^{\dagger\dagger}; c^{\dagger\dagger} < c < c^{**}; c^{**} < c < c^{\dagger}; c^{\dagger} < c < c^*; c > c^*. \tag{4.1}$$

To understand the dynamics of the system (2.4) more comprehensively, we present the stabilities of various equilibriums completely in Table 3, considering that the dynamics of the system also depend on the relationship between threshold E_T and z_{11}, z_{12}, z_{21}, and z_{22}. Thus, we have the following threshold levels:

$$E_T > z_{21}; z_{11} < E_T < z_{21}; z_{12} < E_T < z_{11}; z_{22} < E_T < z_{12}; 0 < E_T < z_{22}. \tag{4.2}$$

Table 3. The stability of equilibrium points for subsystem $\mathbb{S}^1$ and $\mathbb{S}^2$ when $R_0 > R_{c_1} > R_{c_2} > 1$.

Condition	$E_1^1 = E_1^2 = E_1$	E_{11}	E_{12}	E_{21}	E_{22}
$c_4 < c < c_2$	*LAS*	–	–	*LAS*	*US*
$c_2 < c < c^{\dagger\dagger}$	*LAS*	*LAS*	*US*	*LAS*	*US*
$c^{\dagger\dagger} < c < c^{**}$	*LAS*	*LAS*	*US*	*LAS*	*US*
$c^{**} < c < c^{\dagger}$	*US*	*LAS*	*US*	*LAS*	*US*
$c^{\dagger} < c < c^*$	*US*	*LAS*	*US*	*LAS*	–
$c^* < c$	*US*	*LAS*	–	*LAS*	–

4.1.1. *Case* $(a1) : E_T > z_{21}$

In such a case, if equilibriums E_{11}, E_{12}, E_{21}, and E_{22} exist, it can be noted that E_{11} and E_{12} are virtual, whereas E_{21} and E_{22} are real, with E_{21} being *LAS*. We will examine the following six cases in the light of the connections between c and $c_4, c_2, c^{\dagger\dagger}, c^{**}, c^{\dagger}, c^*$.

Subcase (i): Assume $c_4 < c < c_2$, here we know E_1 is *LAS*. Note that equilibria E_{11} and E_{12} do not exist under this scenario. All the orbits in S^1 will reach the switching line $z = E_T$ within a finite amount of time, then firstly enter S^2 and ultimately approach either E_{21} or E_1 [shown in Figure 2(a)], contingent upon their initial positions. Thus, the E_{21} and E_1 are bistable in this particular scenario.

Subcase (ii): Assume $c_2 < c < c^{\dagger\dagger}$, we have immune-free equilibrium E_1 is *LAS* in subsystem $\mathbb{S}^2$. According to Lemma 4.2, there exists $dy/dt < 0$ on the $\Sigma_s^i (i = 1, 2)$ when ET exceeds z_{21}. Therefore, all the orbits of subsystem $\mathbb{S}^1$ will slide from right to left to the (y_{21}, E_T) or (y_{12}, E_T) when they reach the sliding segments, and finally tend to E_{21}. Hence, E_{21} and E_1 are bistable [illustrated in Figure 2(b)].

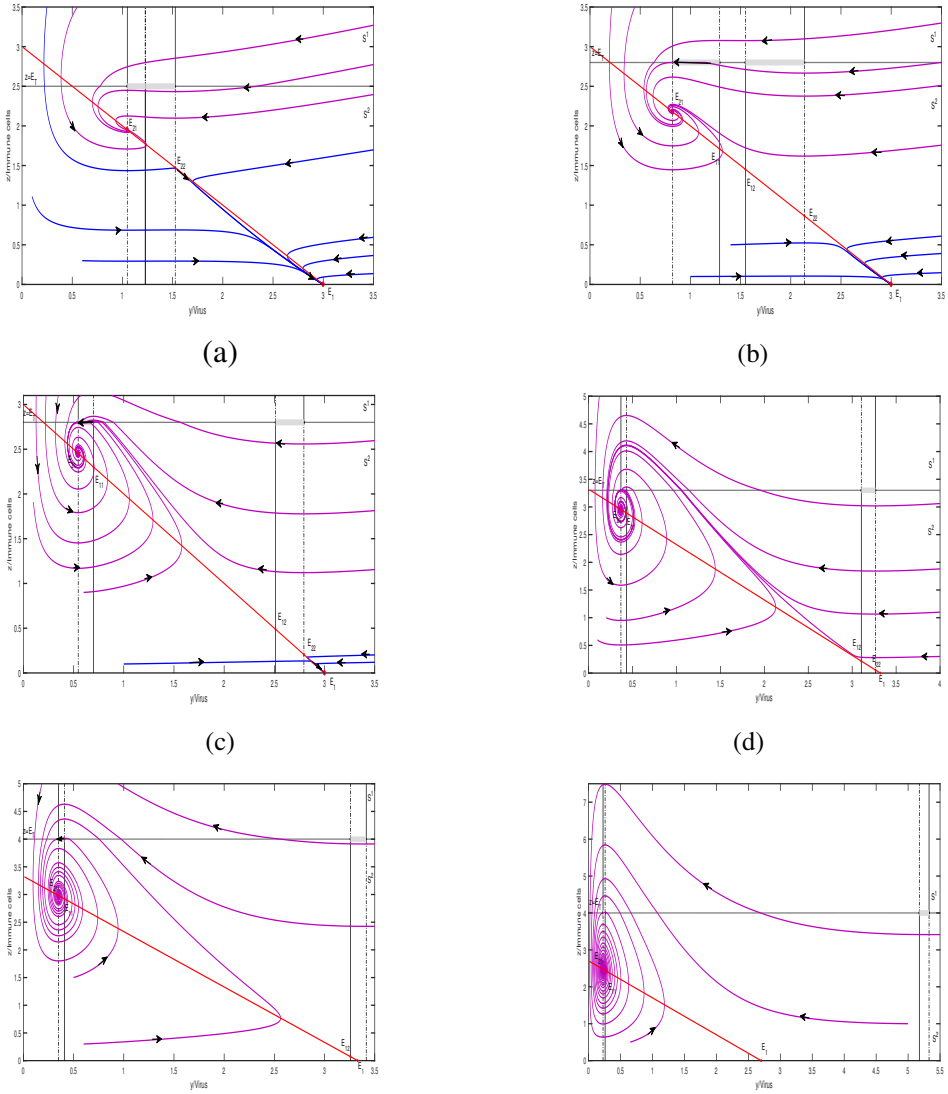

Figure 2. Dynamical behavior of the system (2.4) for $Case(a1)$.

Note: The purple and blue lines represent trajectories that finally tend to the equilibriums E_{21} and E_1, respectively. Parameters are: $r = 6$, $K = 6$, $p = 1$, $q = 1$, $b = 1$ and $(a)\,\eta = 0.55$, $a = 3$, $\varepsilon = 0.12$, $c = 2.9$, $E_T = 2.5$; $(b)\,\eta = 0.5$, $a = 3$, $\varepsilon = 0.12$, $c = 2.92$, $E_T = 2.8$; $(c)\,\eta = 0.57$, $a = 3$, $\varepsilon = 0.13$, $c = 3.4$, $E_T = 2.8$; $(d)\,\eta = 0.75$, $a = 2.68$, $\varepsilon = 0.1$, $c = 4.55$, $E_T = 3.3$; $(e)\,\eta = 0.75$, $a = 2.67$, $\varepsilon = 0.1$, $c = 6.68$, $E_T = 4$; $(f)\,\eta = 0.9$, $a = 3$, $\varepsilon = 0.1$, $c = 6.97$, $E_T = 4$.

Subcase (iii): Assume $c^{\dagger\dagger} < c < c^{**}$, here we have equilibrium E_1, real equilibrium E_{21} are *LAS*. In this subcase, system (2.4) has the same bistable behavior as the previous case [shown in Figure 2(c)].

Subcase (iv): Assume $c^{**} < c < c^{\dagger}$, we get that E_1 is *US*, and there is only one stable equilibrium E_{21}. Thus, any orbit starting from region S^1 firstly crosses the switching line $z = E_T$ and enters S^2, following the dynamics of $\mathbb{S}^2$ tends to E_{21}. Additionally, Lemmas 4.1–4.3 confirms the absence of a limit cycle, implying that all trajectories ultimately converge to E_{21}. Therefore, it can be concluded that the equilibrium E_{21} is *GAS* [shown in Figure 2(d)].

Subcase (v): Assume $c^{\dagger} < c < c^{*}$. In such a subcase, we know equilibrium E_{22} does not exist. In

consideration of the nonexistence of the limit cycle, E_{21} becomes a glocally stable equilibrium [shown in Figure 2(e)].

Subcase (vi): Assume $c > c^*$. Under this scenario, we know equilibria E_{12} and E_{22} do not exist. That is, there exists not any other stable equilibrium other than E_{21}. Considering that the existence of the limit cycle is excluded, endemic equilibrium E_{21} is *GAS* [shown in Figure 2(f)]. The dynamics of the system (2.4) can be summarized below when $E_T > z_{21}$.

Theorem 4.1. *Suppose $E_T > z_{21}$, it can be deduced that both E_{21} and E_1 are bistable for $c_4 < c < c_2, c_2 < c < c^{\dagger\dagger}, c^{\dagger\dagger} < c < c^{**}$; positive equilibrium E_{21} is GAS for $c^{**} < c < c^{\dagger}$, $c^{\dagger} < c < c^*$ and $c > c^*$.*

4.1.2. *Case* $(a2)$: $z_{11} < E_T < z_{21}$

In such a case, if equilibriums E_{11}, E_{12}, E_{21}, and E_{22} exist, we have E_{11}, E_{12}, E_{21} are virtual, while E_{22} is real but *US*. Meanwhile, our analysis reveals the occurrence of sliding mode and the emergence of pseudo-equilibrium within the sliding segment $\Sigma_s^1 = \{(y,z)|\, y_{21} < y < y_{11}, z = E_T\}$. By Theorem 3.1, we know that the pseudo-equilibrium E_c is *LAS* when it exists. Likewise, we will analyze the following six scenarios.

Subcase (i): Assume $c_4 < c < c_2$. We know equilibria E_{11} and E_{12} do not exist, then we have omitted the description for this case.

Subcase (ii): Assume $c_2 < c < c^{\dagger\dagger}$. In such a subcase, E_1 is *LAS* in the subsystem $\mathbb{S}^2$ and the pseudo-equilibrium will appear on the sliding segment Σ_s^1. Thus, the partial orbits starting from region S^1 will follow the dynamics of $\mathbb{S}^1$ to the sliding segment $\{(y,z)|\, y_{21} < y < y_c, z = E_T\}$, whereas partial trajectories starting from subsystem $\mathbb{S}^2$ will arrive at the segment $\{(y,z)|\, y_c < y < y_{11}, z = E_T\}$ along the $\mathbb{S}^2$, depending on the initial point, and both types of orbits will eventually converge toward pseudo-equilibrium E_c. Therefore, we conclude that E_c and E_1 are bistable [shown in Figure 3(a)].

Subcase (iii): Assume $c^{\dagger\dagger} < c < c^{**}$. In such a subcase, we get that both pseudo-equilibrium E_c on the sliding segment Σ_s^1 and equilibrium E_1 are *LAS*. Thus, we can obtain the coincident conclusion by using similar ways of discussion. That is, the orbits will either go to E_c or tend to E_1 along the subsystem $\mathbb{S}^1$ and $\mathbb{S}^2$, respectively [shown in Figure 3(b)].

Subcase (iv): Assume $c^{**} < c < c^{\dagger}$. In such a subcase, E_c is the only stable equilibrium for the system (2.4). Our findings reveal that all trajectories intersecting with the line $z = E_T$ and following the sliding segment Σ_s^1 reach the pseudo-equilibrium E_c. Considering that a limit cycle does not exist for the entire system, we can conclude that E_c is *GAS* [illustrated in Figure 3(c)].

Subcase (v): Assume $c^{\dagger} < c < c^*$. In such a subcase, we know E_{22} does not exist and the pseudo-equilibrium E_c is *LAS*. Here, we have immune-free equilibrium E_1 is *US*. Equally, system (2.4) does not exist any limit cycle. Then the equilibrium E_c is *GAS* [shown in Figure 3(d)].

Subcase (vi): Assume $c > c^*$. Under this condition, equilibria E_{12} and E_{22} do not exist. There is only one stable equilibrium E_c in the switching system (2.4). Considering the exclusion of closed orbit, then E_c is *GAS* [illustrated in Figure 3(e)]. Hence, we summarize the aforementioned conclusion of system (2.4) to the following when $z_{11} < E_T < z_{21}$.

Theorem 4.2. *Suppose $z_{11} < E_T < z_{21}$, we can conclude that system (2.4) has bistable behavior, i.e., immune-free equilibrium E_1 and pseudo-equilibrium E_c are LAS for $c_2 < c < c^{\dagger\dagger}, c^{\dagger\dagger} < c < c^{**}$; equilibrium E_c is GAS for $c^{**} < c < c^{\dagger}$, $c^{\dagger} < c < c^*$ and $c > c^*$.*

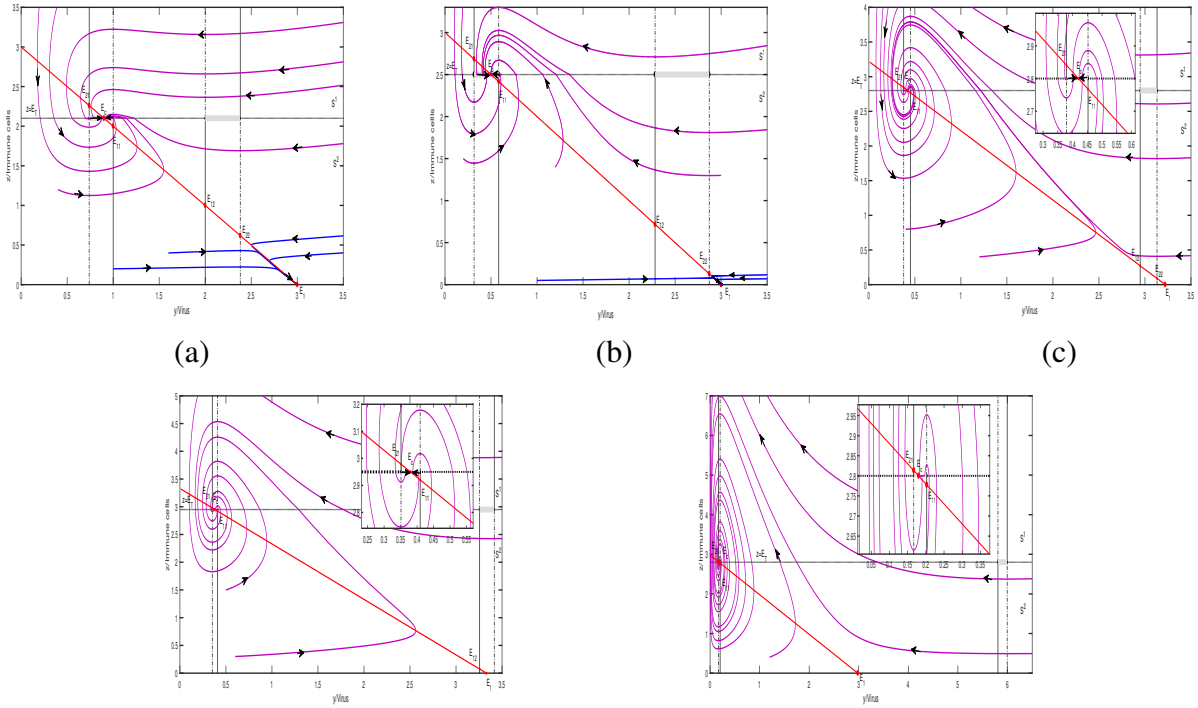

(a) (b) (c)

(d) (e)

Figure 3. Dynamical behavior of the system (2.4) for $Case(a2)$.

Note: The purple and blue lines represent trajectories that finally tend to the equilibriums E_c and E_1, respectively. Parameters are: $r = 6$, $K = 6$, $p = 1$, $q = 1$, $b = 1$ and $(a)\,\eta = 0.5$, $a = 3$, $\varepsilon = 0.12$, $c = 3$, $E_T = 2.1$; $(b)\,\eta = 0.75$, $a = 3$, $\varepsilon = 0.32$, $c = 3.9$, $E_T = 2.5$; $(c)\,\eta = 0.75$, $a = 2.78$, $\varepsilon = 0.11$, $c = 4.48$, $E_T = 2.8$; $(d)\,\eta = 0.75$, $a = 2.67$, $\varepsilon = 0.1$, $c = 6.7$, $E_T = 2.95$; $(e)\,\eta = 0.85$, $a = 3.02$, $\varepsilon = 0.15$, $c = 6.96$, $E_T = 2.8$.

4.1.3. $Case\,(a3)$: $z_{12} < E_T < z_{11}$

In such a case, if equilibriums $E_{11}, E_{12}, E_{21}, E_{22}$ exist, we get E_{12} and E_{21} are virtual, but E_{11} and E_{22} are real, where E_{11} is *LAS* in the $\mathbb{S}^1$. We prove the existence of sliding mode but there is no pseudo-equilibrium. Next, we will analyze the stability of equilibria based on the connections between c and $c_4, c_2, c^{\dagger\dagger}, c^{**}, c^{\dagger}, c^{*}$.

Subcase (i): Assume $c_4 < c < c_2$. Under this scenario, it follows from Section 2 that the two equilibria E_{11} and E_{12} are not feasible. So we can omit the description for this case.

Subcase (ii): Assume $c_2 < c < c^{\dagger\dagger}$. In such a subcase, E_1 is *LAS* and E_{11} is a real and stable equilibrium, since subsystem $\mathbb{S}^1$ has only one stable endemic state. Thus, trajectories initiating from $\mathbb{S}^1$ will intend to approach the equilibrium E_{11}. In this scenario, the endemic equilibrium E_{11} can coexist with the immune-free equilibrium E_1. That is, system (2.4) has bistable behavior [shown in Figure 4(a)].

Subcase (iii): Assume $c^{\dagger\dagger} < c < c^{**}$. Regarding the presence and stability of the equilibriums, the dynamics exhibited by subsystems $\mathbb{S}^1$ and $\mathbb{S}^2$ resemble those of the former scenario [shown in Figure 4(b)]. Thus, we get that E_{11} and E_1 are bistable for the Filippov system (2.4).

Subcase (iv): Assume $c^{**} < c < c^{\dagger}$. In this subcase, the equilibrium E_{21} is virtual and the

system (2.4) only exhibits one stable endemic equilibrium E_{11}. As there is no limit cycle, then E_{11} is GAS [shown in Figure 4(c)].

Subcase (v): Assume $c^{\dagger} < c < c^{*}$. Analogously, there exists only one stable equilibrium point E_{11} in subsystem $\mathbb{S}^1$. It should be noted that the endemic equilibrium E_{11} functions as an attractor. We have excluded the existence of limit cycles. Consequently, any orbit starting from region $\mathbb{S}^1$ or $\mathbb{S}^2$ will approach the equilibrium point E_{11} [shown in Figure 4(d)]. Thus, the equilibrium E_{11} is *GAS*.

Subcase (vi): Assume $c > c^{*}$. In this scenario, since the equilibria E_{12} and E_{22} do not exist, we have omitted the description for this case and we get the following conclusion.

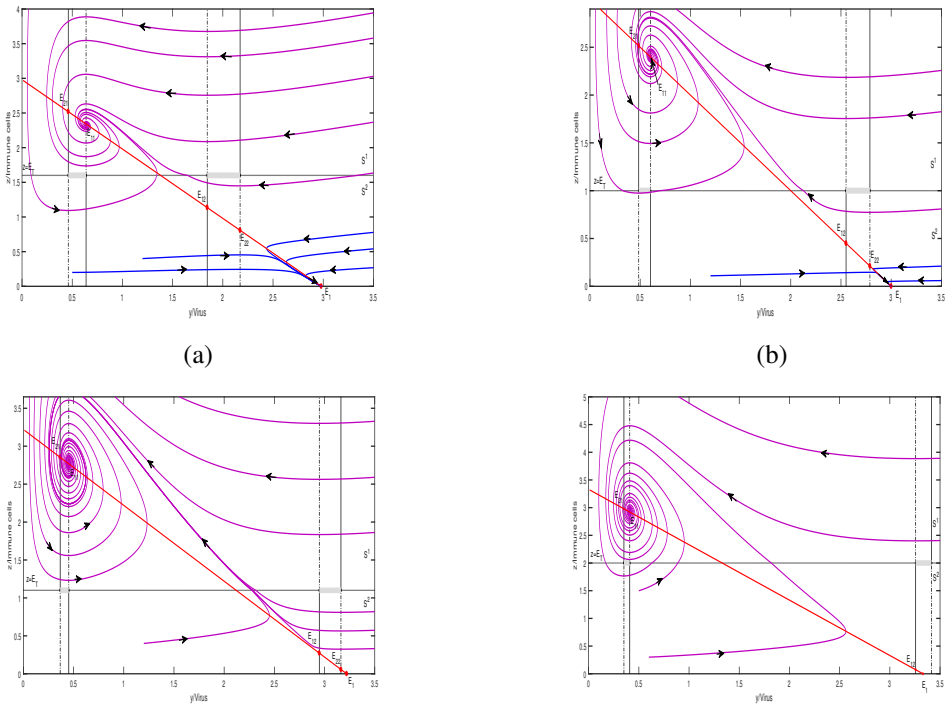

(a) (b)

(c) (d)

Figure 4. Dynamical behavior of the system (2.4) for $Case(a3)$.

Note: The purple and blue lines represent trajectories that finally tend to the equilibriums E_{11} and E_1, respectively. Parameters are: $r = 6$, $K = 6$, $p = 1$, $q = 1$, $b = 1$ and $(a)\,\eta = 0.85$, $a = 3.02$, $\varepsilon = 0.15$, $c = 3.96$, $E_T = 1.6$; $(b)\,\eta = 0.65$, $a = 3$, $\varepsilon = 0.12$, $c = 3.7$, $E_T = 1$; $(c)\,\eta = 0.75$, $a = 2.78$, $\varepsilon = 0.13$, $c = 4.48$, $E_T = 1.1$; $(d)\,\eta = 0.75$, $a = 2.67$, $\varepsilon = 0.1$, $c = 6.7$, $E_T = 2$.

Theorem 4.3. *Suppose $z_{12} < E_T < z_{11}$, we can conclude that immune-free equilibrium E_1 and endemic equilibrium E_{11} are bistable for $c_2 < c < c^{\dagger\dagger}$ and $c^{\dagger\dagger} < c < c^{**}$; equilibrium E_{11} is GAS for $c^{**} < c < c^{\dagger}$ and $c^{\dagger} < c < c^{*}$.*

4.1.4. *Case* $(a4)$: $z_{22} < E_T < z_{12}$

In such a case, if equilibriums E_{11}, E_{12}, E_{21}, and E_{22} exist, we have E_{21} is virtual, while E_{11}, E_{12}, and E_{22} are real. Note that both equilibriums E_{12} and E_{22} are US. Furthermore, the sliding mode does exist, and the pseudo-equilibrium E_c is *LAS* on the Σ_s^2. A similar discussion works for $z_{22} < E_T < z_{12}$.

Subcase (i): Assume $c_4 < c < c_2$, we know equilibria E_{11} and E_{12} do not exist according to Section 2. Therefore, we can ignore the explanation of this situation.

Subcase (ii): Assume $c_2 < c < c^{\dagger\dagger}$. In such a subcase, E_1 is *LAS* and E_{11} is real and stable in $\mathbb{S}^1$. As mentioned above, the pseudo-equilibrium E_c is *LAS*. From the dynamics of subsystems $\mathbb{S}^2$ and $\mathbb{S}^1$, it can be deduced that the orbits will either directly reach the E_{11}, E_1 or firstly arrive at the line $z = E_T$ on the segment $\{(y,z)|\, y_{12} < y < y_{22}, z = E_T\}$, then slide to the E_c along sliding segment Σ_s^2, depending on the initiating points. Hence, as is shown in Figure 5(a), the equilibriums E_{11}, E_c, and E_1 are tristable.

Subcase (iii): Assume $c^{\dagger\dagger} < c < c^{**}$. In such a subcase, we get that the equilibrium E_1 is *LAS*, and there exist two equilibria E_{11} and E_c, which are locally stable in their respective regions. Thus, we can conclude that the dynamic behaviors in this scenario are consistent with the former subcase. That is, system (2.4) has tristable behavior in this case [shown in Figure 5(b)].

Subcase (iv): Assume $c^{**} < c < c^{\dagger}$. Note that the locally stable equilibrium E_{21} is virtual, then cannot be attained. Part of the trajectories starting from subsystem $\mathbb{S}^1$ will approach the equilibrium E_{11}, while certain trajectories will collide on the switching line at finite time, and the locally stable pseudo-equilibrium E_c appears ultimately on the segment $\Sigma_s^2 = \{(y,z)|\, y_{12} < y < y_{22}, z = E_T\}$. Hence, they are bistable for the switching system (2.4) [shown in Figure 5(c)].

Subcase (v): Assume $c^{\dagger} < c < c^{*}$. We know equilibrium E_{22} does not exist, then we rule this out.

Subcase (vi): Assume $c > c^{*}$. In such a subcase, we know equilibria E_{12} and E_{22} do not exist, so we have omitted the description in this case as well. To sum up, we can derive the conclusion as follows.

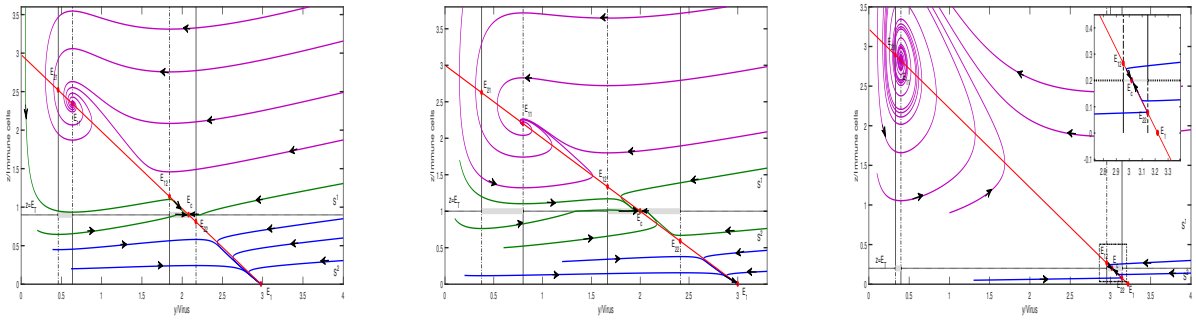

(a) (b) (c)

Figure 5. Dynamical behavior of the system (2.4) for *Case*$(a4)$.

Note: The trajectories represented by the purple, green, and blue lines finally tend to the equilibrium points E_{11}, E_c, and E_1, respectively. Parameters are: $r = 6$, $K = 6$, $p = 1$, $q = 1$, $b = 1$, and (a) $\eta = 0.85$, $a = 3.02$, $\varepsilon = 0.15$, $c = 3.96$, $E_T = 0.9$; (b) $\eta = 0.75$, $a = 3$, $\varepsilon = 0.32$, $c = 3.6$, $E_T = 1$; (c) $\eta = 0.85$, $a = 2.78$, $\varepsilon = 0.12$, $c = 4.9$, $E_T = 0.2$.

Theorem 4.4. *Suppose $z_{22} < E_T < z_{12}$, we can conclude that the real equilibrium E_{11}, pseudo-equilibrium E_c, and the immune-free equilibrium E_1 are tristable for $c_2 < c < c^{\dagger\dagger}$ and $c^{\dagger\dagger} < c < c^{**}$; immune-free equilibrium E_{11} and pseudo-equilibrium E_c are bistable for $c^{**} < c < c^{\dagger}$.*

4.1.5. *Case*$(a5)$: $0 < E_T < z_{22}$

In such a case, if equilibriums E_{11}, E_{12}, E_{21}, and E_{22} exist, we have E_{21} and E_{22} are virtual, but E_{11}, E_{12} are real, where E_{11} is *LAS* in the $\mathbb{S}^1$. Under this scenario, there is no pseudo-equilibrium for the Filippov system (2.3). Subsequently, we will analyze the following situations based on the relationships between immune intensity c and $c_4, c_2, c^{\dagger\dagger}, c^{**}, c^{\dagger}, c^{*}$.

Subcase (i): Assume $c_4 < c < c_2$. In this condition, we get that equilibria E_{11} and E_{12} do not exist on the basis of the discussion of Section 2. Note that the locally stable equilibrium E_{21} is virtual. Thus, there is not any other stable equilibrium besides E_1, as all the possible limit cycles have been excluded. Hence, we have E_1 is *GAS* [shown in Figure 6(a)].

Subcase (ii): Assume $c_2 < c < c^{\dagger\dagger}$. In such a subcase, E_1 is *LAS* and E_{11} is a real and stable equilibrium. However, E_{21} is virtual in $\mathbb{S}^1$. Thus, positive equilibrium E_{11} and immune-free equilibrium E_1 are bistable for $c_2 < c < c^{\dagger\dagger}$ being satisfied [shown in Figure 6(b)].

Subcase (iii): Assume $c^{\dagger\dagger} < c < c^{**}$. We know that equilibria E_{11} and E_1 are *LAS* as well. Thus, the dynamics of this case are similar to the former, i.e., the bistable behavior occurs [shown in Figure 6(c)].

Subcase (iv): Assume $c^{**} < c < c^{\dagger}$. In such a subcase, note that locally stable equilibrium E_{21} is virtual and then cannot be attained. There exists only one stable equilibrium point E_{11} in subsystem $\mathbb{S}^1$. As there is no limit cycle, we obtain that the equilibrium E_{11} is *GAS* [illustrated in Figure 6(d)].

Subcase (v): Assume $c^{\dagger} < c < c^{*}$. In such a subcase, we know that equilibrium E_{22} does not exist, so we have ignored the description of this situation.

Subcase (vi): Assume $c > c^{*}$. In such a subcase, both E_{12} and E_{22} do not exist, therefore, the explanation for this case is omitted. Consequently, we arrive at the subsequent conclusion.

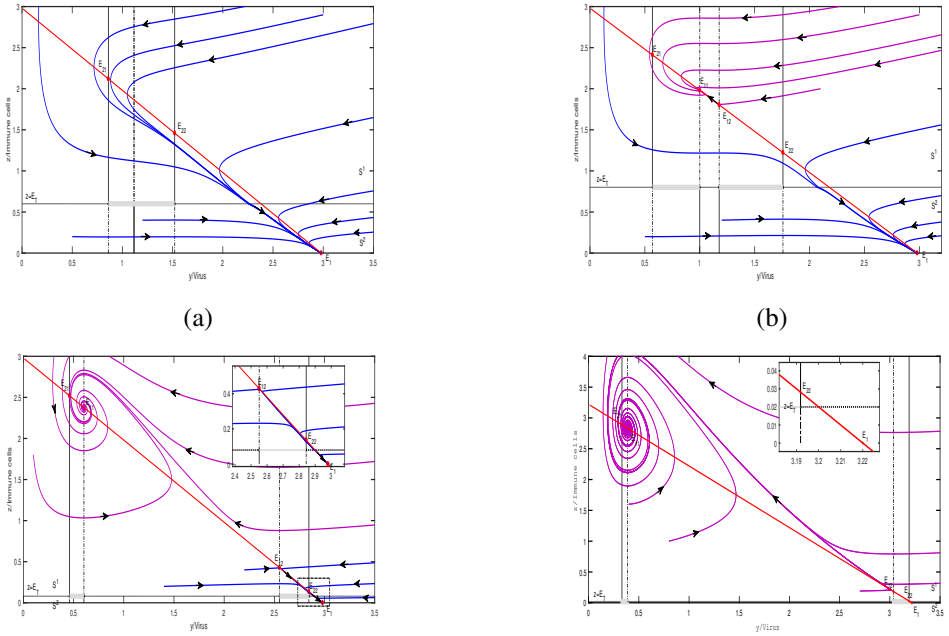

(a) (b) (c) (d)

Figure 6. Dynamical behavior of the system (2.4) for $Case(a5)$.

Note: The purple and blue lines represent trajectories that finally tend to the equilibriums E_{11} and E_1, respectively. Parameters are: $r = 6$, $K = 6$, $p = 1$, $q = 1$, $b = 1$, and $(a)\,\eta = 0.65$, $a = 3.02$, $\varepsilon = 0.15$, $c = 3.1$, $E_T = 0.6$; $(b)\,\eta = 0.85$, $a = 3.02$, $\varepsilon = 0.15$, $c = 3.7$, $E_T = 0.8$; $(c)\,\eta = 0.65$, $a = 3.02$, $\varepsilon = 0.15$, $c = 3.7$, $E_T = 0.08$; $(d)\,\eta = 0.75$, $a = 2.78$, $\varepsilon = 0.13$, $c = 4.5$, $E_T = 0.04$.

Theorem 4.5. *Suppose* $0 < E_T < z_{22}$, *we can conclude that immune-free equilibrium* E_1 *is GAS for* $c_4 < c < c_2$; *the real equilibrium* E_{11} *and immune-free equilibrium* E_1 *are bistable for* $c_2 < c < c^{\dagger\dagger}$ *and* $c^{\dagger\dagger} < c < c^{**}$; *the equilibrium* E_{11} *is GAS for* $c^{**} < c < c^{\dagger}$.

In fact, extensive discussions have been conducted on the stability of various equilibriums for the switching system (2.4) under Case(a). Furthermore, Table 4 provides a comprehensive summary of the global dynamics associated with these specific cases.

5. Boundary equilibrium bifurcation

Notably, the collision of pseudo-equilibrium, tangent point, and regular equilibrium (or tangent point and regular equilibrium) in switching systems occurs when E_T reaches a critical value, leading to boundary equilibrium bifurcations on the discontinuity surface [as shown in Figure 7]. The understanding and analysis of these boundary equilibrium bifurcations are crucial in studying the dynamical behavior of the Filippov system. To verify the boundary equilibrium bifurcation, we select E_T as the bifurcation parameter while keeping all other parameters constant. Detailed explanations of the boundary equilibrium and the tangent point are shown in Definitions 2.3 and 2.5.

Boundary equilibrium of the Filippov system (2.4) satisfies

$$ry\left(1-\frac{y}{K}\right)-ay-pyz=0,\frac{cyz}{1+\eta y}-bz-qyz+\phi\varepsilon z=0,z-E_T=0, \tag{5.1}$$

where $\phi=0$ or $\phi=1$. By solving the equations provided in (5.1), it is possible to obtain four potential boundary equilibria

$$E_B^{11}=(y_{11},E_T),E_B^{12}=(y_{12},E_T),E_B^{21}=(y_{21},E_T),E_B^{22}=(y_{22},E_T). \tag{5.2}$$

Tangent points of the Filippov system (2.4) satisfy

$$\frac{cyz}{1+\eta y}-bz-qyz+\phi\varepsilon z=0,z-E_T=0. \tag{5.3}$$

Thus, the potential tangent points can be denoted as

$$T_{11}=(y_{11},E_T),T_{12}=(y_{12},E_T),T_{21}=(y_{21},E_T),T_{22}=(y_{22},E_T), \tag{5.4}$$

which are the solutions of (5.4) corresponding to $\phi=0$ and $\phi=1$.

Figure 7 examines a series of boundary equilibrium bifurcations when $c_2<c<c^{\dagger\dagger}$. In this case, both subsystems have two positive equilibria. The real and stable equilibrium E_{21} coexists simultaneously with the visible tangent point T_{21} when $E_T>z_{21}$ [shown in Figure 7(a)]. As E_T decreases from $E_T>z_{21}$ to z_{21}, E_{21} collides with T_{21} [shown in Figure 7(b)]. With the threshold E_T decreasing further to $z_{11}<E_T<z_{21}$, a stable pseudo-equilibrium E_c emerges and T_{21} transforms into an invisible tangent point [as depicted in Figure 7(c)]. This bifurcation exhibits the progress of the formation of E_c. Furthermore, boundary bifurcation takes place again when E_T through the critical value z_{11}. This case results in the collision of the tangent point T_{11}, the equilibrium point E_{11} with the pseudo-equilibrium point E_c [as depicted in Figure 7(d)]. Subsequently, the E_c vanishes, and the stable point E_{11} transforms into the local attractor [as illustrated in Figure 7(e)]. When E_T drops consistently until z_{12}, the third boundary bifurcation takes place, leading to the collision of the visible tangent point T_{12} with the equilibriums E_{12} [as depicted in Figure 7(f)].

Table 4. Existence and stability of the equilibria for the Filippov system (2.4) when $R_0 > R_{c_1} > R_{c_2} > 1$.

Threshold value	Immune intensity	E_1	E_{11}	E_{12}	E_{21}	E_{22}	E_c	Global stability
$E_T > z_{21}$	$c_4 < c < c_2$	LAS	$-$	$-$	$LAS(R)$	US	$-$	Bistable
	$c_2 < c < c^{\dagger\dagger}$	LAS	$LAS(V)$	US	$LAS(R)$	US	$-$	Bistable
	$c^{\dagger\dagger} < c < c^{**}$	LAS	$LAS(V)$	US	$LAS(R)$	US	$-$	Bistable
	$c^{**} < c < c^{\dagger}$	US	$LAS(V)$	US	$LAS(R)$	US	$-$	E_{21} GAS
	$c^{\dagger} < c < c^{*}$	US	$LAS(V)$	US	$LAS(R)$	$-$	$-$	E_{21} GAS
	$c^{*} < c$	US	$LAS(V)$	$-$	$LAS(R)$	$-$	$-$	E_{21} GAS
$z_{11} < E_T < z_{21}$	$c_2 < c < c^{\dagger\dagger}$	LAS	$LAS(V)$	US	$LAS(V)$	US	LAS	Bistable
	$c^{\dagger\dagger} < c < c^{**}$	LAS	$LAS(V)$	US	$LAS(V)$	US	LAS	Bistable
	$c^{**} < c < c^{\dagger}$	US	$LAS(V)$	US	$LAS(V)$	US	LAS	E_c GAS
	$c^{\dagger} < c < c^{*}$	US	$LAS(V)$	US	$LAS(V)$	$-$	LAS	E_c GAS
	$c^{*} < c$	US	$LAS(V)$	$-$	$LAS(V)$	$-$	LAS	E_c GAS
$z_{12} < E_T < z_{11}$	$c_2 < c < c^{\dagger\dagger}$	LAS	$LAS(R)$	US	$LAS(V)$	US	$-$	Bistable
	$c^{\dagger\dagger} < c < c^{**}$	LAS	$LAS(R)$	US	$LAS(V)$	US	$-$	Bistable
	$c^{**} < c < c^{\dagger}$	US	$LAS(R)$	US	$LAS(V)$	US	$-$	E_{11} GAS
	$c^{\dagger} < c < c^{*}$	US	$LAS(R)$	US	$LAS(V)$	$-$	$-$	E_{11} GAS
$z_{22} < E_T < z_{12}$	$c_2 < c < c^{\dagger\dagger}$	LAS	$LAS(R)$	US	$LAS(V)$	US	LAS	Tristable
	$c^{\dagger\dagger} < c < c^{**}$	LAS	$LAS(R)$	US	$LAS(V)$	US	LAS	Tristable
	$c^{**} < c < c^{\dagger}$	US	$LAS(R)$	US	$LAS(V)$	US	LAS	Bistable
$0 < E_T < z_{22}$	$c_4 < c < c_2$	LAS	$-$	$-$	$LAS(V)$	US	$-$	E_1 GAS
	$c_2 < c < c^{\dagger\dagger}$	LAS	$LAS(R)$	US	$LAS(V)$	US	$-$	Bistable
	$c^{**} < c < c^{\dagger}$	US	$LAS(R)$	US	$LAS(V)$	US	$-$	E_{11} GAS

The real equilibrium and virtual equilibrium are represented by R and V, respectively.

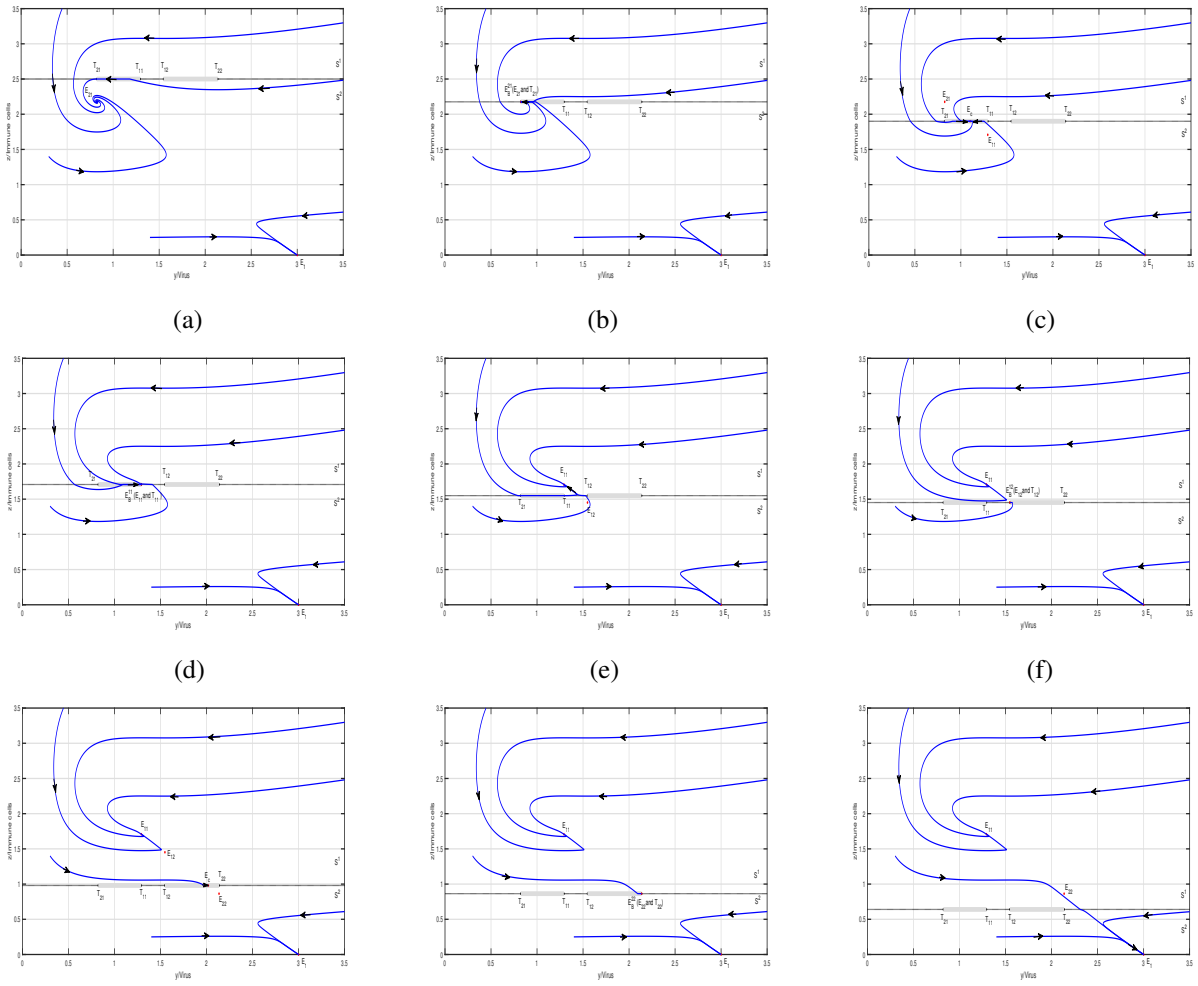

Figure 7. Boundary equilibrium bifurcations for the switching system (2.4).

Note: Here, we choose E_T as a bifurcation parameter and other parameter values are fixed as $r = 6$, $K = 6$, $p = 1$, $q = 1$, $b = 1$, $\eta = 0.5$, $a = 3$, $\varepsilon = 0.12$, $c = 2.92$ and (a) $E_T = 2.5$; (b) $E_T = 2.176$; (c) $E_T = 1.9$; (d) $E_T = 1.7081$; (e) $E_T = 1.55$; (f) $E_T = 1.4519$; (g) $E_T = 0.98$; (h) $E_T = 0.864$; (i) $E_T = 0.64$.

Provided E_T continues to decrease until $z_{22} < E_T < z_{12}$, a locally stable pseudo-equilibrium E_c appears [as shown in Figure 7(g)] and a tristable phenomenon (E_c, E_{11}, and the immune-free equilibrium E_1) occurs. When E_T passes E_{22}, the fourth boundary equilibrium bifurcation occurs. In this scenario, the pseudo-equilibrium E_c will collide with the equilibrium point E_{22} and tangent point T_{22} if $E_T = z_{22}$ [illustrated in Figure 7(h)]. However, as the threshold E_T continues to decrease, the equilibrium E_c disappears, and the tangent point T_{22} becomes invisible [illustrated in Figure 7(i)]. Here, the equilibriums E_1 and E_{11} exhibit bistability under this scenario.

6. The influence of the pivotal parameters of the system (2.4)

In order to stabilize the HIV viral loads and effector cell counts within the required predetermined level, it is crucial to implement a control strategy for the switching system (2.4) by setting an

appropriate threshold E_T. The dynamics of the system are influenced by two key parameters: The immune intensity c and the inhibition of the virus on the proliferation of immune cells η. Therefore, it is important to study the impact of these parameters on the system's dynamics. Note that the parameters in this study are based on the findings of Komarova [33] and colleagues. A direct calculation reveals that the bistable interval is (2.7666,3.2333) [shown in Figure 8(a)]. From this figure, it is evident that system (2.4) has the potential to have either one or two nontrivial *LAS* equilibria depending on the value of c. In detail, two stable equilibriums E_1^2 and E_{21} coexist when $c_4 < c < c^{\dagger\dagger}$. As established in Section 2, there is a unique *LAS* equilibrium E_{21} if $c > c^{\dagger\dagger}$. It is important to note that a saddle-node bifurcation occurs at $c = c_4$. Generally, a longer bistable interval implies a wider range of variation for the proliferation coefficient c of immune cells. In this context, a lower viral inhibition intensity η [shown in Figure 8(b)] is more advantageous for immune control. This indicates the necessity of developing medications aimed at diminishing the viral inhibitory effect on immune cells. The phase portrait of this system reveals that both variables y and z will gradually tend to a stable value over time t changed [shown in Figures 8(c) and (d)]. In subsystem $\mathbb{S}^2$, the combination of antiretroviral therapy and immunotherapy not only controlled the number of viruses better but also stabilized the immune cell count at a more reliable level than the free system, as can be seen in Figures 8(e) and (f).

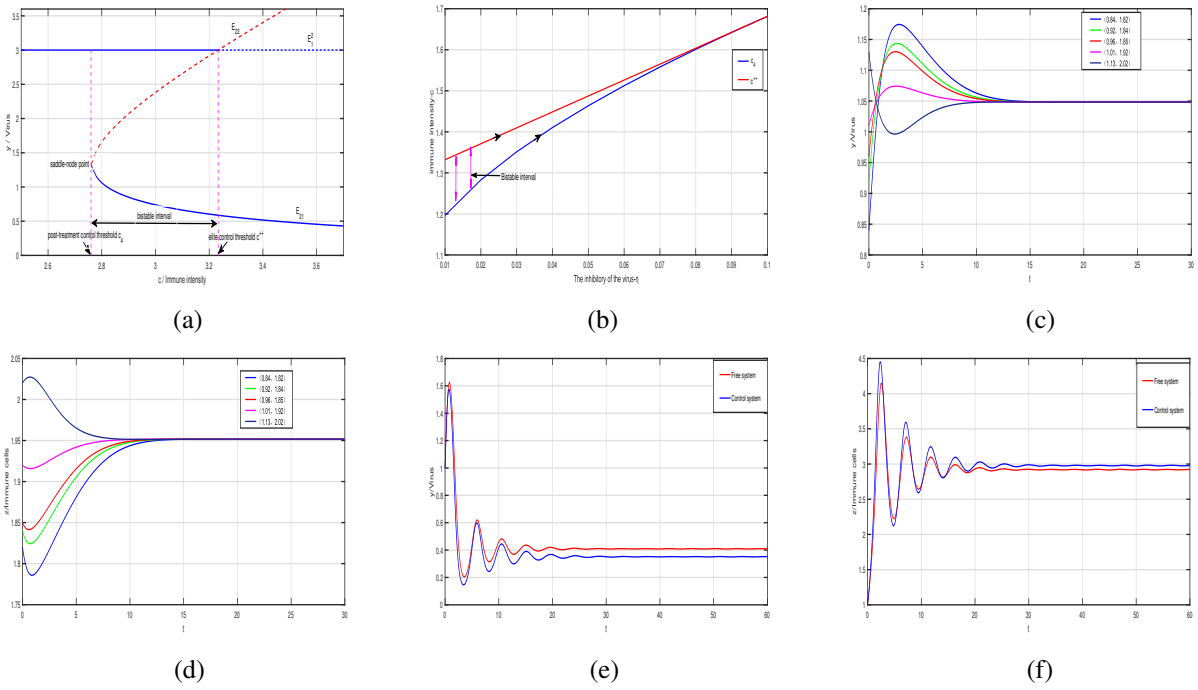

Figure 8. (a) Saddle–node bifurcation diagram and bistable of the subsystem $\mathbb{S}^2$, where $r = 6$, $K = 6$, $p = 1$, $q = 1$, $b = 1$, $\eta = 0.5$, $a = 3$, $\varepsilon = 0.12$ such that $c_2 = 2.7666$, $c^{\dagger\dagger} = 3.2333$, where the *LAS* equilibrium of viral load is depicted by the solid line, while the dashed line illustrates the *US* equilibrium; (b) The impact of the intensity of virus inhibition (η) on the duration of the bistable interval; (c) and (d) Parameters are $\eta = 0.55$, $a = 3$, $\varepsilon = 0.12$, $c = 2.9$, the other parameter values are the same to those of (a). At this point, the system will gradually tend to stabilize; (e) and (f) The dynamic behaviors of virus and immune cells in the system (2.4) within time.

7. Conclusions

Given the immunosuppressive HIV infection model [32–34], it is suggested that the threshold policy control (TPC) method for treating infected patients should be based on the number of immune cells. Thus, we propose a piecewise immunosuppressive infection system. We call model (2.4) a discontinuous right-hand side dynamical system under TPC, which consists of two subsystems. Specifically, it is recommended to initiate a combination of antiretroviral therapy and immune therapy when the value drops below a certain threshold E_T, which includes the usage of antiretroviral medications and interleukin (IL)-2. This leads to the emergence of a nonsmooth system. Unlike [31], we consider the logical growth of HIV rather than linear growth in this paper. Some clinical facts indicate that the saturated growth of HIV is reasonable.

Initially, we provide a concise overview of the dynamics exhibited by the two subsystems. Through the subsystems $\mathbb{S}^i (i = 1, 2)$, we derive the thresholds R_0, R_{c_1}, and R_{c_2}. It becomes evident that R_0 plays a pivotal part in determining the eradication of the virus. We also obtain the post-treatment control thresholds $c_2(c_4)$ and the elite control threshold $c^{**}(c^{\dagger\dagger})$ for subsystems $\mathbb{S}^1$ ($\mathbb{S}^2$). According to [34], there exists a bistable behavior between these two threshold intervals. The sliding dynamics and sliding domain of the system (2.4) are studied in the subsequent analysis. Our purpose is to demonstrate the existence of two sliding segments $\Sigma_s^i (i = 1, 2)$. By employing the Filippov convex approach, we investigate the possibility and local asymptotic stability of the pseudo-equilibrium E_c on the sliding segment Σ_s^1 under the $z_{11} < E_T < z_{21}$, or on the sliding segment Σ_s^2 under the $z_{22} < E_T < z_{12}$. Significantly, we have primarily focused on Case (a) and discussed the global dynamics of the system in this paper. To investigate the global dynamic behavior of the system, we have excluded the existence of three types of limit cycles. It is important to understand the relationship not only among R_0, R_{c_1}, R_{c_2}, and 1 but also among immune intensity c and $c_4, c_2, c^{\dagger\dagger}, c^{**}, c^{\dagger}, c^*$. Subsequently, the bifurcation theories were utilized to address the dynamics of sliding mode and local sliding bifurcations.

The analysis reveals that the system can demonstrate diverse and complex dynamic behaviors: (i) One of the equilibria in the system is *GAS*, which can manifest as the immune-free equilibrium E_1, pseudo-equilibrium E_c, or even as the positive equilibrium E_{11} or E_{21} within subsystems $\mathbb{S}^1$ or $\mathbb{S}^2$; (ii) There are two possible equilibria in this system that exhibit bistability, namely the immune-free equilibrium E_1 and equilibrium E_{21} (or E_c or E_{11}), or the positive equilibrium E_{11}, which is bistable alongside the pseudo-equilibrium E_c; (iii) Three equilibria are tristable, i.e., immune-free equilibrium E_1, positive equilibrium E_{11}, and the pseudo-equilibrium E_c are stable for $z_{22} < E_T < z_{12}$ and $c_2 < c < c^{**}$. Our work demonstrates that the utilization of effector cell-guided therapy leads to an expansion of the controllable area of initial values for patients, generating a more complex Filippov dynamics system when compared with [35]. Interestingly, we find that there exists an optimal threshold interval for immune intensity that can maximize the controllable area of initial values. This highlights the importance of considering the effects of effector cell-guided therapy and immune intensity when studying the dynamics of the switching system. It suggests that maximizing the controllable area of initial values can potentially improve the effectiveness of treatment strategies for patients.

In this paper, the existence of three types of equilibria including pseudo-equilibrium is explored. These equilibria can exhibit bistability or tristability, meaning that the HIV viral loads and effector cell counts can be stabilized at a preset level. Achieving these stable states depends on factors such as the threshold level, immune intensity, and the initial values of the system. Consequently, determining

the optimal strategy for immune intensity and the threshold conditions should still take into account the individual characteristics of the patients. In the case of boundary $H(X)$, the selection of parameter values is crucial in stabilizing different equilibria within the system. From a biological standpoint, employing rational control intensity and intervention is highly effective in ensuring the control and management of diseases.

Although our research has an impact on HIV disease control, it is still insufficient. We only consider the relationship between the number of effector cells and the threshold level to construct switching conditions. The actual disease control strategy should also take into account the change rate of effector cell count, which will be our next work. By considering these factors, we aim to further provide insights into the effectiveness and impact of this treatment approach on the virus-immune system dynamics. This mathematical model could potentially contribute to the improvement of treatment strategies for viral infections.

Use of AI tools declaration

The authors declare that no Artificial Intelligence (AI) tools were used in the creation of this article.

Acknowledgments

This work was supported by The National Natural Science Foundation of China (Grant No. 12261033).

The authors would like to thank the editor and anonymous referees for their valuable comments and suggestions, which have led to an improvement of the paper.

Conflict of interest

The authors declare no conflict of interest.

References

1. A. A. Alderremy, J. F. Gómez-Aguilar, S. Aly, K. M. Saad, A fuzzy fractional model of coronavirus (COVID-19) and its study with Legendre spectral method, *Results. Phys.*, **21** (2021), 103773. http://dx.doi.org/10.1016/j.rinp.2020.103773
2. P. Pandey, Y. M. Chu, J. F. Gómez-Aguilar, H. Jahanshahi, A. A. Aly, A novel fractional mathematical model of COVID-19 epidemic considering quarantine and latent time, *Results. Phys.*, **26** (2021), 104286. http://dx.doi.org/10.1016/j.rinp.2021.104286
3. A. A. Khan, R. Amin, S. Ullah, W. Sumelka, M. Altanji, Numerical simulation of a Caputo fractional epidemic model for the novel coronavirus with the impact of environmental transmission, *Alex. Eng. J.*, **61** (2022), 5083–5095. http://dx.doi.org/10.1016/j.aej.2021.10.008
4. S. Kumar, A. Ahmadian, R. Kumar, D. Kumar, J. Singh, D. Baleanu, et al., An efficient numerical method for fractional SIR epidemic model of infectious disease by using Bernstein wavelets, *Mathematics*, **8** (2020), 558. http://dx.doi.org/10.3390/math8040558

5. M. S. Abdo, K. Shah, H. A. Wahash, Sa. K. Panchal, On a comprehensive model of the novel coronavirus (COVID-19) under Mittag-Leffler derivative, *Chaos. Solition. Fract.*, **135** (2020), 109867. http://dx.doi.org/10.1016/j.chaos.2020.109867
6. F. J. Palella, K. M. Delaney, A. C. Moorman, M. O. Loveless, J. Fuhrer, G. A. Satten, et al., Declining morbidity and mortality among patients with advanced human immunodeficiency virus infection, *N. Engl. J. Med.*, **338** (1998), 853–860. http://dx.doi.org/10.1056/nejm199803263381301
7. A. Mocroft, S. Vella, T. L. Benfield, A. Chiesi, V. Miller, P. Gargalianos, et al., Changing patterns of mortality across Europe in patients infected with HIV-1, *The Lancet*, **352** (1998), 1725–1730. http://dx.doi.org/10.1016/s0140-6736(98)03201-2
8. M. P. Davenport, D. S. Khoury, D. Cromer, S. R. Lewin, A. D. Kelleher, S. J. Kent, Functional cure of HIV: The scale of the challenge, *Nat. Rev. Immunol.*, **19** (2019), 45–54. http://dx.doi.org/10.1038/S41577-018-0085-4
9. Z. Meng, Y. Chen, M. Lu, Advances in targeting the innate and adaptive immune systems to cure chronic hepatitis B virus infection, *Front. Immunol.*, **10** (2020), 3127. http://dx.doi.org/10.3389/fimmu.2019.03127
10. L. Zhang, B. Ramratnam, K.Tenner-Racz, Y. He, M. Vesanen, S. Lewin, et al., Quantifying residual HIV-1 replication in patients receiving combination antiretroviral therapy, *N. Engl. J. Med.*, **340** (1999), 1605–1613. http://dx.doi.org/10.1056/NEJM199905273402101
11. A. Carr, K. Samaras, A. Thorisdottir, G. R. Kaufmann, D. J. Chisholm, D. A. Cooper, diagnosis, prediction, and natural course of HIV-1 protease-inhibitor-associated lipodystrophy, hyperlipidaemia, and diabetes mellitus: a cohort study, *The Lanc.*, **353** (1999), 2093–2099. http://dx.doi.org/10.1016/S0140-6736(98)08468-2
12. M. Shahzad, H. Chen, T. Akhtar, A. Rafi, M. S. Zafar, Y. T. Zheng, Human immunodeficiency virus: The potential of medicinal plants as antiretroviral therapy, *J. Med. Virol*, **94** (2022), 2669–2674. http://dx.doi.org/10.1002/jmv.27648
13. Y. Xiao, S. Tang, Y. Zhou, R. J. Smith, J. Wu, N. Wang, Predicting the HIV/AIDS epidemic and measuring the effect of mobility in mainland China, *J. Theor. Biol.*, **317** (2013), 271–285. http://dx.doi.org/10.1016/j.jtbi.2012.09.037
14. Z. Wang, X. Q. Zhao, A Within-Host virus model with periodic multidrug therapy, *B. Math. Biol.*, **75** (2013), 543–563. http://dx.doi.org/10.1007/s11538-013-9820-y
15. A. Jarne, D. Commenges, L. Villain, M. Prague, Y. Lévy, R. Thiébaut, Modeling CD4 + T cells dynamics in HIV-infected patients receiving repeated cycles of exogenous Interleukin 7, *Ann. Appl. Stat.*, **11** (2017), 1593–1616. http://dx.doi.org/10.1214/17-AOAS1047
16. C. C. Espitia, M. A. Botina, M. A. Solarte, I. Hernandez, R. A. Riascos, J. F. Meyer, Mathematical model of HIV/AIDS considering sexual preferences under antiretroviral therapy, a case study in san juan de pasto, colombia, *J. Comput. Biol.*, **29** (2022), 483–493. http://dx.doi.org/10.1089/cmb.2021.0323
17. P. K. Roy, A. N. Chatterjee, D. Greenhalgh, Q. J. A. Khan, Long term dynamics in a mathematical model of HIV-1 infection with delay in different variants of the basic drug therapy model, *Nonlinear Anal. RWA*, **14** (2013), 1621–1633. http://dx.doi.org/10.1016/j.nonrwa.2012.10.021

18. Y. Jao, N. Erawaty, Dynamic study of the pathogen-immune system interaction with natural delaying effects and protein therapy, *AIMS Math.*, **7** (2022), 7471–7488. http://dx.doi.org/10.3934/math.2022419

19. N. Erawaty, N. Aris, A mathematical study of effects of delays arising from the interaction of anti-drug antibody and therapeutic protein in the immune response system, *AIMS Math.*, **5** (2020), 7191–7213. http://dx.doi.org/10.3934/math.2020460

20. Y. C. Yan, W. D. Wang, Global stability of a five-dimensional model with immune responses and delay, *Discrete Cont. Dyn.-B*, **17** (2017), 401–416. http://dx.doi.org/10.3934/dcdsb.2012.17.401

21. W. L. Duan, L. Lin, Noise and delay enhanced stability in tumor-immune responses to chemotherapy system, *Chaos, Soliton. Fract.*, **148** (2021), 111019. http://dx.doi.org/10.1016/j.chaos.2021.111019

22. H. Shu, L. Wang, Joint impacts of therapy duration, drug efficacy and time lag in immune expansion on immunity boosting by antiviral therapy, *J. Biol. Syst.*, **25** (2017), 105–117. http://dx.doi.org/10.1142/s0218339017500061

23. K. F. Wang, W. D. Wang, S. P. Song, Dynamics of an HBV model with diffusion and delay, *J. Theor. Biol.*, **253** (2008), 36–44. http://dx.doi.org/10.1016/j.jtbi.2007.11.007

24. W. Wang, X. N. Wang, Z. S. Feng, Time periodic reaction–diffusion equations for modeling 2-LTR dynamics in HIV-infected patients, *Nonlinear Anal. RWA*, **57** (2021), 103184. http://dx.doi.org/10.1016/j.nonrwa.2020.103184

25. Q. Ge, X. Wang, L. Rong, A delayed reaction-diffusion viral infection model with nonlinear incidences and cell-to-cell transmission, *Int. J. Biomath.*, **8** (2021), 14. http://dx.doi.org/10.1142/S179352452150100X

26. F. Maggiolo, M. Airoldi, A. Callegaro, C. Martinelli, A. Dolara, T. Bini, et al., CD4 cell-guided scheduled treatment interruptions in HIV-infected patients with sustained immunologic response to HAART, *AIDS*, **23** (2009), 799–807. http://dx.doi.org/10.1097/qad.0b013e328321b75e

27. S. Arshad, D. Baleanu, J. Huang, Y. Tang, M. M. Al Qurashi, Dynamical analysis of fractional order model of immunogenic tumors, *Adv. Mech. Eng.*, **8** (2016). http://dx.doi.org/10.1177/1687814016656704

28. Y. N. Xiao, H. Y. Miao, S. Y. Tang, H. L. Wu, Modeling antiretroviral drug responses for HIV-1 infected patients using differential equation models, *Adv. Drug. Deliv. Rev.*, **65** (2013), 940–953. http://dx.doi.org/10.1016/j.addr.2013.04.005

29. L. B. Rong, Z. L. Feng, A. S. Perelson, Emergence of HIV-1 drug resistance during antiretroviral treatment, *B. Math. Biol.*, **69** (2007), 2027–2060. http://dx.doi.org/10.1007/s11538-007-9203-3

30. S. Tang, Y. Xiao, N. Wang, H. Wu, Piecewise HIV virus dynamic model with CD4+ T cell count-guided therapy: I, *J. Theor. Biol.*, **308** (2012), 123–134. http://dx.doi.org/10.1016/j.jtbi.2012.05.022

31. B. Tang, Y. N. Xiao, S. Sivaloganathan, J. H. Wu, A piecewise model of virus-immune system with effector cell-guided therapy, *Appl. Math. Model.*, **47** (2017), 227–248. http://dx.doi.org/10.1016/j.apm.2017.03.023

32. H. Shu, L. Wang, J. Watmough, Sustained and transient oscillations and chaos induced by delayed antiviral immune response in an immunosuppressive infection model, *J. Math. Biol.*, **68** (2013), 477–503. http://dx.doi.org/10.1007/s00285-012-0639-1

33. N. L. Komarova, E. Barnes, P. Klenerman, D. Wodarz, Boosting immunity by antiviral drug therapy: A simple relationship among timing, efficacy, and success, *Proc. Natl. Acad. Sci.*, **100** (2003), 1855–1860. http://dx.doi.org/10.1073/pnas.0337483100

34. S. L. Wang, F. Xu, Thresholds and bistability in virus-immune dynamics, *Appl. Math. Lett.*, **78** (2018), 105–111. http://dx.doi.org/10.1016/j.aml.2017.11.002

35. M. D. Bernardo, C. J. Budd, A. R. Champneys, P. Kowalczyk, A. B. Nordmark, G. O. Tost, et al., Bifurcations in nonsmooth dynamical systems, *SIAM Rev.*, **50** (2008), 629–701. http://dx.doi.org/10.1137/050625060

36. M. Guardia, T. M. Seara, M. A. Teixeira, Generic bifurcations of low codimension of planar Filippov systems, *J. Differ. Equ.*, **250** (2011), 1967–2023. http://dx.doi.org/10.1016/j.jde.2010.11.016

37. W. Qin, S. Tang, The selection pressures induced non-smooth infectious disease model and bifurcation analysis, *Chaos. Solition. Fract.*, **69** (2014), 160–171. http://dx.doi.org/10.1016/j.chaos.2014.09.014

38. Y. Zhang, Y. Xiao, Global dynamics for a Filippov epidemic system with imperfect vaccination, *Nonlinear Anal. Hybri.*, **38** (2020), 100932. http://dx.doi.org/10.1016/j.nahs.2020.100932

AIMS Press